JOURNAL OF PETROLOGY | VOLUME 51 | NUMBERS 1 & 2 | PAGES 201–227 | 2010 | doi:10.1093/petrology/egp077

Composition and Genesis of Depleted Mantle Peridotites from the Wadi Tayin Massif, Oman Ophiolite; Major and Trace Element Geochemistry, and Os Isotope and PGE Systematics

KAREN HANGHØJ[1]*, PETER B. KELEMEN[1], DEBORAH HASSLER[2] AND MARGUERITE GODARD[3]

[1]LAMONT DOHERTY EARTH OBSERVATORY OF COLUMBIA UNIVERSITY, PO BOX 1000, PALISADES, NY 10964, USA
[2]STATOIL GULF OF MEXICO LLC, BUILDING 4, 9TH FLOOR, 2101 CITY WEST BOULEVARD, HOUSTON, TX 77042, USA
[3]GÉOSCIENCES MONTPELLIER, UMR 5243 CNRS-UM2, UNIVERSITÉ MONTPELLIER 2, CC60, PLACE E. BATAILLON, 34095 MONTPELLIER CEDEX 5, FRANCE

RECEIVED JANUARY 6, 2009; ACCEPTED OCTOBER 28, 2009

The Oman ophiolite consists of several massifs cropping out along a 500 km long band trending NW–SE along the coast of Oman; it is one of the best exposed sections of oceanic crust and mantle in the world. There is a gradient in igneous processes and composition in the ophiolite, with the northern massifs recording a polygenetic igneous history involving an increasingly important subduction component, whereas the southern massifs were formed primarily via a mid-ocean ridge basalt (MORB)-like, single-stage process at a submarine spreading ridge. In this study we use geochemical data from Wadi Tayin, which is one of the southern massifs of the Oman ophiolite, to constrain the composition and genesis of oceanic crust and upper mantle. The Wadi Tayin harzburgites are residues of partial melting that are as depleted as the most depleted mid-ocean ridge peridotites. They have low middle- to heavy rare earth element ratios, most probably reflecting melting close to and beyond the exhaustion of clinopyroxene. Like many abyssal peridotites, the Wadi Tayin samples show enrichment in highly incompatible elements, giving rise to U-shaped MORB-normalized trace element patterns. We favor the idea that this is caused by enrichment of highly incompatible elements along grain boundaries in peridotite, which may be the result of near-equilibrium partitioning between grain boundaries and grain interiors, rather than disequilibrium processes. Equilibrium partitioning between crystals and grain boundaries during melting and melt extraction is also our preferred explanation for ubiquitous high Pb contents relative to Ce and La in our samples as well as in most abyssal peridotites. The Wadi Tayin samples record substantial variability in terms of osmium isotopic composition and platinum group element (PGE) concentrations. The more radiogenic nature of the dunites and impregnated peridotites compared with the residual harzburgites may be due to relatively high $^{187}Os/^{188}Os$ in melt transported through the dunites. The presence of residual peridotites with whole-rock osmium isotopic compositions less radiogenic than MORB may be explained by melting of a veined (upwelling) mantle forming mixed melts in which much of the Os derives from veins with high Re/Os in a matrix of previously depleted peridotite. An important result of this study is that the shallowest samples are refertilized (i.e. anomalously enriched in incompatible elements), and record relatively high metamorphic closure temperatures. These observations suggest that migrating melt underwent crystallization during rapid cooling in the uppermost mantle during and immediately after ridge magmatism. A variety of geothermometers all yield the result that the stratigraphically highest harzburgites equilibrated at higher temperature than the deeper ones. The systematic decrease in closure temperature with increasing depth below the Moho transition zone probably reflects systematic variation in cooling rate as a function of depth in the

*Corresponding author. Present address: Woods Hole Oceanographic Institution, Geology and Geophysics, MS# 23, Woods Hole, MA 02543, USA. E-mail: khanghoj@whoi.edu

© The Author 2010. Published by Oxford University Press. All rights reserved. For Permissions, please e-mail: journals.permissions@oxfordjournals.org

mantle section. We hypothesize that the refertilization and higher closure temperatures recorded by the uppermost mantle samples are linked. More rapid cooling led to higher closure temperatures, and to partial crystallization of migrating melts in the shallowest part of the mantle section, yielding slightly elevated abundances of elements such as Ca and Na, and incompatible trace elements.

KEY WORDS: *mantle peridotites; Oman ophiolite; geothermometry; osmium isotopes*

INTRODUCTION

The Oman ophiolite (Fig. 1) provides complete sections through the igneous crust and the uppermost mantle formed at an oceanic spreading center. The presence of pillow basalts underlain by a continuous layer of sheeted dikes demonstrates that the crust formed at a submarine spreading center. The Oman ophiolite has long been a focus of study because of its excellent exposures over a large area, and the geochemical similarity between Oman samples and mid-ocean ridge samples. The compositional similarities between residual peridotite, gabbro and lavas from Oman and from mid-ocean ridges indicate that magmatic processes are similar in both settings (e.g. Pallister, 1981; Pallister & Knight, 1981). Major and trace element equilibrium between primitive lavas, sheeted dikes, primitive lower crustal gabbros and dunite melt conduits in the residual mantle section show that all are part of a co-genetic package formed at the spreading ridge (e.g. Kelemen & Dick, 1995; Kelemen *et al.*, 1997), as confirmed by Nd isotope data (McCulloch *et al.*, 1981; Sharma & Wasserburg, 1996).

This study focuses on samples from the mantle section of the southernmost massif of the Oman ophiolite, the Wadi Tayin massif. This massif consists of an extensive mantle section overlain by a 5–7 km thick crustal gabbro section and a nearly continuous layer of dikes and pillow lavas (Fig. 1) (e.g. Boudier & Coleman, 1981; Pallister & Hopson, 1981). The crust–mantle boundary in the Wadi Tayin massif dips 20–30° to the south (Boudier & Coleman, 1981; Pallister & Hopson, 1981; Nicolas & Boudier, 2001) and the underlying mantle section extends for 20–30 km north of this contact. Thus, it is inferred that the mantle section of the Wadi Tayin massif has a structural thickness of more than 10 km.

The Samail massif, just to the west, has a generally flat-lying crust–mantle transition (Nicolas *et al.*, 2000), and so the depth extent of the mantle exposures is limited; the structural thickness of mantle peridotites is largest in the NE corner of the Samail massif, where it may reach 3 or 4 km. We have made detailed studies of mantle peridotites in this NE corner of the Samail massif (Wadi Lufti), just 10 km from the NW corner of the Wadi Tayin massif (Braun & Kelemen, 2002; Braun, 2004) and some data from those studies are incorporated into this work.

The mantle section of both the Wadi Tayin and Samail massifs is composed of residual harzburgite and minor lherzolite that host 5–15% discordant dunite (Boudier & Coleman, 1981). The dunites occur as tabular veins and sheets with sharp contacts, ranging in width from <1 cm to 100 m or more (Kelemen *et al.*, 1997; Braun & Kelemen, 2002). The harzburgites are residues of partial melting and melt extraction, and are geochemically similar to the more depleted end of the abyssal peridotite compositional spectrum (Boudier & Coleman, 1981; Gregory, 1984; Kelemen *et al.*, 1995; Godard *et al.*, 2000). The dunites represent chemically isolated channels of focused melt transport through the harzburgites and were formed by melt–rock reaction between mid-ocean ridge basalt (MORB)-like melts and harzburgite (e.g. Kelemen *et al.*, 1995, 1997; Braun & Kelemen, 2001, 2002; Braun, 2004).

This study presents major and trace element, mineral and Os isotope analyses for a set of samples of dunite and harzburgite from the Wadi Tayin massif, spanning an estimated stratigraphic thickness of more than 10 km, with the objective of investigating spatial variability in the mantle section and of constraining upper mantle processes of melting and melt transport.

THE OMAN OPHIOLITE

The Oman ophiolite consists of several massifs cropping out along a 500 km long band trending NW–SE along the coast of Oman. It is one of the best exposed sections of oceanic crust and mantle in the world (Fig. 1). On the basis of radiometric age data, crustal thickness, a general lack of paleo-fracture zones, a nearly continuous layer of gabbro between volcanic and mantle rocks, and other geological observations, it is probable that it formed at a medium- to fast-spreading ridge like the East Pacific Rise (EPR) or the Juan de Fuca Ridge (e.g. Tilton *et al.*, 1981; Nicolas, 1989). For summaries of previous work on the Oman ophiolite, the reader is referred to Pallister & Knight (1981), Pearce *et al.* (1981), Alabaster *et al.* (1982), Lippard *et al.* (1986), Lorand & Ceuleneer (1989), Ildefonse *et al.* (1993), Nicolas *et al.* (1994, 1996, 2000), Kelemen *et al.* (1995, 1997), Nicolas & Boudier (1995), Hacker *et al.* (1996), Holtzman *et al.* (2000), Braun & Kelemen (2002), Takazawa *et al.* (2003), Arai *et al.* (2004) and Monnier *et al.* (2006).

Volcanic rocks are best exposed in the northern massifs of the ophiolite; there the main lava series, the Geotimes and Lasail volcanics, are tholeiitic basalts and andesites. The lower Geotimes series lavas have rare earth element (REE) and trace element contents similar to MORB (e.g. Alabaster *et al.*, 1982; Godard *et al.*, 2003). However, they also include andesites and dacites, which are rare among mid-ocean ridge lavas (e.g. Pearce *et al.*, 1981).

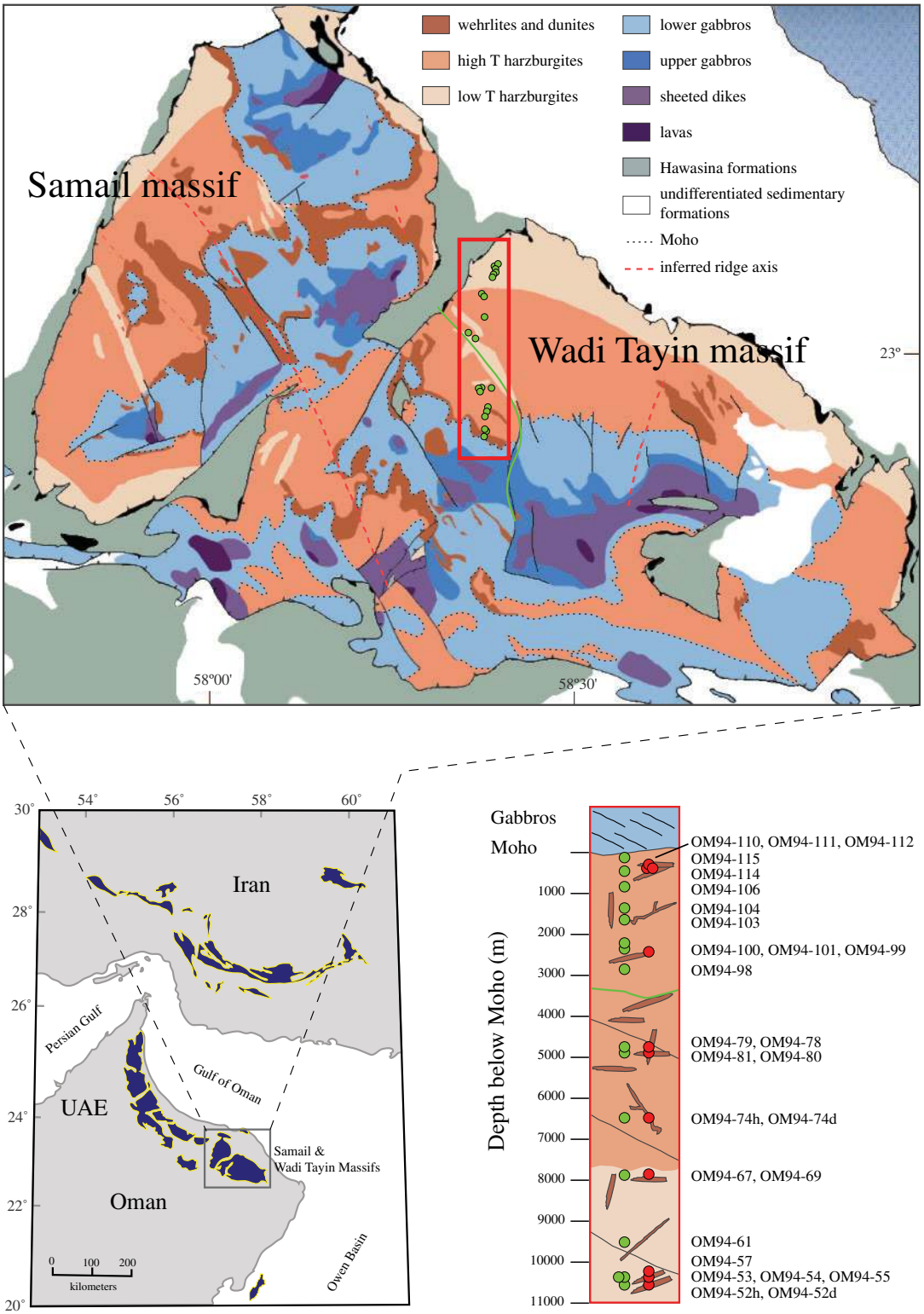

Fig. 1. Geological map of the Samail and Wadi Tayin massifs, Oman ophiolite, from Nicolas *et al.* (2000) showing the study area in the Wadi Tayin mantle section (red rectangle); sample locations are shown by green circles. Schematic cross-section of same sample transect is also shown with inferred sample depths; harzburgite samples are shown as green circles, dunite samples as red circles. The green line dissecting the sample area is the location of the Makhibiyah shear zone from Nicolas & Boudier (2008).

The younger Lasail lavas, which overlie the Geotimes series in the northern massifs, are depleted in REE relative to MORB and are geochemically similar to lavas found above some subduction zones (Pearce *et al.*, 1981; Alabaster *et al.*, 1982; Lippard *et al.*, 1986; Ernewein *et al.*, 1988; Ishikawa *et al.*, 2002), although isotopically the Lasail lavas are indistinguishable from the Geotimes lavas (Godard *et al*, 2003). Also in the northern massifs, primitive, orthopyroxene-rich gabbronorites and pyroxenites are abundant in the lower crust and as intrusions into shallow mantle peridotites (Smewing, 1981; Juteau *et al.*, 1988*a*, 1988*b*; Reuber, 1988; Reuber *et al.*, 1991; Lachize *et al.*, 1996; Boudier *et al.*, 2000), consistent with the presence of depleted, primitive andesite magmas. Such primitive, orthopyroxene-rich cumulates are rare among oceanic samples. 'Wehrlitic' intrusions and pyroxenites are also present in the mantle and lower crustal gabbros and their genesis has been extensively discussed (Juteau, 1988; Juteau *et al.*, 1988; Reuber, 1988, 1991). True wehrlites and pyroxenites are rare or absent among samples of crust formed at mid-ocean ridges.

Finally, spinel in mantle harzburgite and dunite in the northern massifs has molar Cr-number [$100 \times (Cr/(Cr+Al)$] greater than 75 (e.g. Lippard *et al.*, 1986; Augé, 1987; Ahmed & Arai, 2002; Araihich *et al.*, 2004), unlike that in oceanic peridotite samples, in which spinel consistently has a Cr-number less than 70 (Dick & Bullen, 1984).

The southern massifs of the Oman ophiolite, commonly known as the Samail and Wadi Tayin (or Ibra) massifs, lack many of the features listed above, which distinguish the northern massifs from crust and residual mantle formed at mid-ocean ridges. In the southern massifs, some lavas have trace element characteristics that are identical to MORB, whereas others lie just outside the MORB field on discriminant plots (e.g. Pallister & Knight, 1981; Braun, 2004). Primitive gabbroic rocks in the lower crust of the two massifs do not contain orthopyroxene (e.g. Pallister & Hopson, 1981; Korenaga & Kelemen, 1997; Kelemen *et al.*, 1997; Garrido *et al.*, 2001; Koga *et al.*, 2001). Peridotites have spinel Cr-numbers that generally overlap the more depleted end of the range for dredged oceanic mantle samples (e.g. Braun, 2004). Residual harzburgites record 'near fractional' partial melt extraction and are geochemically similar to abyssal peridotites (Kelemen *et al.*, 1995; Godard *et al.*, 2000; Le Mée *et al.*, 2004; Monnier *et al.*, 2006). Dunites within the mantle section represent channels of focused melt transport through the harzburgites, and were formed by melt–rock reaction between MORB-like melts and harzburgite (Kelemen *et al.*, 1995; Braun & Kelemen, 2002; Braun, 2004).

In the Samail and Wadi Tayin massifs small, late-stage websterite and gabbronorite intrusions are rare and confined to the mantle section (e.g. Boudier & Coleman, 1981; Amri *et al.*, 1996; Benoit *et al.*, 1996; Kelemen *et al.*, 1997; Python & Ceuleneer, 2003). Such orthopyroxene-rich cumulates may be correlative with small gabbronorite intrusions into peridotite dredged and drilled at mid-ocean ridges (Ross & Elthon, 1993; Benoit *et al.*, 1999; Nonnotte *et al.*, 2005). Lower crustal 'wehrlites' in the southern Oman massifs are all, or almost all, melanocratic (plagioclase-poor) olivine gabbros. Pallister & Hopson (1981) did show a photomicrograph of a plagioclase-free wehrlite, but despite extensive sampling from the same outcrop, and elsewhere in the Samail and Wadi Tayin massifs, we have been unable to recover any plagioclase-free wehrlites. Pallister & Hopson (1981) emphasized that true wehrlites are rare in the southern Oman ophiolite and estimated that melanocratic gabbro intrusions make up about 5% of the crustal section in the Wadi Tayin massif.

In summary, the southern massifs of the Oman ophiolite are relatively similar to mid-ocean ridges, unlike the northern massifs. Thus, we hypothesize that there is a gradient in igneous processes and composition of the Oman ophiolite as previously suggested by Godard *et al.* (2003), with the northern massifs recording a polygenetic igneous history involving an increasingly important subduction component, whereas the southern massifs were formed primarily via a MORB-like, single-stage process at a submarine spreading ridge. Thus, we use geochemical data from the southern massifs of the Oman ophiolite to constrain the composition and genesis of oceanic crust and mantle.

There remain some differences between the southern massifs and normal spreading ridges, particularly the slightly high Th/Nb and SiO_2 in some Wadi Tayin lavas, and slightly high spinel Cr-number in some Wadi Tayin peridotites compared with mid-ocean ridge samples. Whether or not the southern massifs of the Oman ophiolite were formed at a 'normal' mid-ocean ridge (Braun, 2004), in a suprasubduction-zone setting, or via the unique processes of ophiolite obduction is still uncertain, but we believe resolving this question is not of great importance in applying observations from the southern Oman massifs to constraining igneous processes at oceanic spreading centres.

SAMPLES AND ANALYTICAL METHODS

The mantle section of the Wadi Tayin massif was sampled along a NNE–SSW transect covering its entire structural thickness, which is more than 10·5 km. For this study, 27 samples of harzburgite and dunite were analyzed for major and trace element concentrations, Os isotopic composition and platinum group element (PGE) concentrations. Most samples have also been analyzed for their constituent mineral compositions. Depth below the Moho is estimated from the strike and dip of the Moho and the distance to the Moho, and is listed in Table 1 along with

Table 1: Bulk-rock major and trace element compositions of harzburgites and dunites

Sample:	OM94-52h	OM94-53	OM94-54	OM94-61	OM94-67	OM94-74h	OM94-79	OM94-81	OM94-98	OM94-100	OM94-101
Lithology:	harzburgite	harzburgite	harzburgite	harzburgite	harzburgite	harzburgite	harzburgite	harzburgite	harzburgite	harzburgite	harzburgite
Mineralogy:	ol, opx, sp	ol, opx, sp	ol, opx, sp	ol, opx, sp	ol, opx, sp	ol, opx, sp	ol, opx, sp	ol, opx, sp, ≪cpx	ol, opx, sp	ol, opx, sp	ol, opx, sp
UTM E:	642454	641962	641962	641722	640273	640617	638436	639361	641651	639879	640053
UTM N:	2556170	2555850	2555850	2554460	2551773	2548967	2546829	2546074	2539355	2539328	2539043
Depth below Moho (m):	10550	10325	10325	9595	7860	6430	4895	4910	2880	2200	2150
wt %											
SiO_2	38·77	39·01	37·85	38·90	40·43	40·63	40·12	39·03	41·30	39·60	41·12
TiO_2	0·017	0·016	0·018	0·018	0·017	0·018	0·017	0·014	0·012	0·011	0·010
Al_2O_3	0·86	0·63	0·67	0·70	1·01	0·90	0·94	0·56	0·76	0·59	0·68
FeO^*	6·99	7·10	7·78	6·65	7·32	7·11	7·52	7·74	7·74	7·38	7·70
MnO	0·114	0·115	0·120	0·103	0·116	0·117	0·120	0·122	0·122	0·121	0·125
MgO	39·21	40·85	41·73	40·73	40·93	40·08	40·34	41·16	41·38	41·23	40·63
CaO	0·99	0·80	0·81	0·40	1·14	1·27	1·07	0·68	0·72	0·78	0·96
Na_2O	0·09	0·11	0·11	0·10	0·08	0·09	0·08	0·09	0·09	0·09	0·09
K_2O	0·00	0·01	0·00	0·01	0·00	0·00	0·00	0·00	0·00	0·00	0·00
P_2O_5	0·010	0·012	0·010	0·010	0·010	0·009	0·010	0·010	0·009	0·009	0·009
Cr_2O_3	0·357	0·374	0·470	0·362	0·352	0·371	0·398	0·393	0·330	0·272	0·354
LOI	11·67	9·85	9·81	11·26	8·03	8·83	8·44	9·84	7·56	8·49	7·85
Total	99·08	98·87	99·37	99·24	99·45	99·43	99·06	99·64	100·03	98·58	99·53
Mg-no.	90·92	91·12	90·54	91·61	90·88	90·95	90·54	90·46	90·51	90·88	90·40
ppm											
Li	0·64	0·8	0·8	1·07	0·8	1	0·67	0·62	0·7	0·63	0·52
Sc	10·8	8·9	7·4	6·0	9·9	10·9	9·9	9·0	9·7	10·8	11·1
Ti	69·9	39·3	56·8	59·9	69·2	76·3	64·2	53·0	39·2	41·3	24·6
Co	112	110	117	100	109	106	103	109	109	121	110
Ni	2241	2234	2255	20·88	2196	2122	2036	2222	2166	2516	2234
Cu	10·2	18·0	24·1	8·6	11·2	18·7	16·4	25·6	11·0	7·0	23·9
ppb											
Rb	12·1	9·7	9·0	33·8	16·3	26·9	15·4	14·1	32·7	7·4	6·8
Sr	212	256	412	701		149	43	491	4582	317	1780
Y	183·2	122·9	177·9	111·3	271·6	249·4	193·0	111·7	93·4	108·9	72·2
Zr	8·4	25·5	50·5	16·6	19·3	24·9	32·6	42·8	38·7	75·9	46·8
Nb	12·6	14·0	16·6	8·5	14·0	16·4	13·8	13·3	20·5	10·1	9·8
Cs	2·1	1·9	1·9	8·1	5·7	11·3	4·6	3·4	1·4	2·4	1·7
Ba	18·6	241·9	226·2	73·8			17·8	77·7	147·9		133·5
La			0·7			2·2	2·8	1·2		3·2	3·3
Ce	0·9	2·0	4·6	1·6	1·3	3·1	1·6	2·7	3·2	4·0	3·0
Pr	0·4	0·7	1·3	0·6	0·7	0·8	0·5	0·7	0·6	1·1	0·4
Nd	2·8	4·9	9·1	4·7	5·4	5·6	4·0	5·0		6·4	3·2
Sm								2·3			
Eu	1·3		2·6			2·2	1·4	0·9		1·7	
Gd	7·9	8·1	15·1	6·0	15·1	14·1	8·8	6·4	4·4	7·5	2·9
Tb	2·4	2·0	3·7	1·6	4·5	3·8	2·8	1·6	1·1	1·7	0·7
Dy	27·2	18·9	29·7	16·2	40·8	39·7	27·7	18·0	12·7	16·3	8·8
Ho	8·8	5·9	8·5	5·4	12·7	11·8	8·8	5·4	4·5	5·1	3·5
Er	34·1	23·4	30·8	21·9	48·2	42·9	35·3	21·6	20·4	20·0	15·5
Tm	6·8	4·5	5·1	4·2	9·4	8·0	6·8	4·1	4·4	4·3	3·6
Yb	53·4	36·2	41·6	33·4	70·2	63·2	55·4	35·4	39·3	35·9	33·8
Lu	11·1	7·8	8·5	6·8	14·3	12·9	11·4	7·5	9·2	7·7	7·0
Hf	2·0	2·6	4·9	3·3	3·7	3·4	2·1	2·4	0·9	3·4	2·1
Ta	1·0		1·8	1·1		0·7	0·9	0·6	0·7	0·7	0·4
Pb	18·6			18·3		14·4	15·4	17·8	20·3	20·0	14·4
Th	1·1	0·9	1·2	1·6	1·4	0·9	0·8	0·9	1·1	0·7	0·8
U		1·9	2·3	2·0	1·6	1·0	1·0	0·8		1·3	0·9

(continued)

Table 1: Continued

Sample:	OM94-103[1]	OM94-104	OM94-106	OM94-114[1]	OM94-115[1]	OM94-52d[1]	OM94-55	OM94-57	OM94-69	OM94-74d
Lithology:	harzburgite	harzburgite	harzburgite	harzburgite	harzburgite	dunite	dunite	dunite	dunite	dunite
Mineralogy:	ol, opx, sp	ol, opx, sp	ol, opx, sp	ol, opx, sp	ol, opx, sp	ol, sp	ol, sp	ol, sp, ≪cpx	ol, sp, ≪cpx	ol, sp
UTM E:	641233	641147	640868	640995	640737	642454	641962	642065	640480	640617
UTM N:	2536790	2536242	2535461	253518	2532768	2556170	2555850	2555575	2551773	2548967
Depth below Moho (m):	1652	1390	970	520	45	10550	10325	10220	7795	6430
wt %										
SiO_2	42·22	42·06	42·18	39·46	39·63	32·92	36·39	36·04	36·35	36·77
TiO_2	0·011	0·012	0·014	0·025	0·008	0·013	0·007	0·008	0·009	0·009
Al_2O_3	0·76	0·87	0·83	1·38	0·48	0·96	0·23	0·18	0·19	0·29
FeO*	7·96	7·45	6·92	8·34	7·66	7·67	7·71	7·91	7·13	8·43
MnO	0·129	0·124	0·123	0·129	0·123	0·119	0·114	0·120	0·115	0·127
MgO	41·39	40·24	40·07	41·25	42·06	39·84	44·38	43·79	44·76	44·41
CaO	0·92	0·94	2·28	1·03	0·66	0·10	0·25	0·18	0·19	0·20
Na_2O	0·09	0·09	0·09	0·09	0·10	0·13	0·10	0·10	0·10	0·09
K_2O	0·00	0·00	0·00	0·00	0·00	0·00	0·00	0·00	0·00	0·00
P_2O_5	0·010	0·009	0·010	0·011	0·010	0·012	0·010	0·010	0·009	0·010
Cr_2O_3	0·393	0·409	0·398	0·301	0·393	1·477	0·199	0·299	0·343	0·444
LOI	6·48	7·21	6·48	7·43	8·49	15·46	10·54	11·66	10·45	9·04
Total	100·36	99·42	99·40	99·45	99·62	98·71	99·93	100·30	99·64	99·82
Mg-no.	90·27	90·59	91·17	89·82	90·73	90·26	91·12	90·81	91·80	90·38
ppm										
Li	0·59	0·4	0·54	2·20	0·80	0·08	0·60	0·40	0·58	0·46
Sc	11·0	11·6	13·6	8·2	9·4	4·2	4	4·4	4·5	4·8
Ti	32·2	40·4	39·3	105·9	18·3	53·6	10·3	20·3	23·8	26·9
Co	107	103	95	111·00	118·00	114	122	122	119	129
Ni	2202	2052	2022	2085	2359	2230	2521	2375	2586	2452
Cu	27·7	15·0	10·8	15·9	9·4	7·8	1·4	3·6	2·3	24·1
ppb										
Rb	6·25	11·63	7·33	17·35	6·61	28·3	4·4	6·5	7·6	6·5
Sr	3071	543	656	4705		9949	91		16	41
Y	88·56	86·71	218·82	475·61	57·40	10·0	42·9	43·5	45·1	40·7
Zr	61·4	17·06	32·08	229·95	57·54	11·0	10·1	26·0	24·4	17·7
Nb	9·95	9·26	8·74	9·88	8·43	13·6	15·6	14·5	10·8	15·2
Cs	3·47	9·26	2·55	9·66	1·50	1·8	1·6	1·7	1·5	1·8
Ba	122·22	47·82	46·41	354·23		111			177	39
La	4·03			12·85	1·55	0·8			0·4	1·0
Ce	10·31	0·44	1·05	24·97	5·62	2·2	1·7	3·0	2·9	2·0
Pr	1·63	0·16	0·35	4·28	1·08	0·4	0·6	0·9	1·1	0·5
Nd	8·19			21·85	6·29	2·6	4·4	6·2	8·1	3·3
Sm										
Eu	1·32		2·02	5·66			1·2	1·4		0·6
Gd	4·93	3·14	11·6	33·42			5·0	5·1	5·2	2·8
Tb	1·2	0·76	3·43	9·32	1·17		1·1	1·0	1·0	0·6
Dy	11·62	9·45	34·16	75·61	9·53	2·0	8·6	8·1	8·3	6·3
Ho	4·1	3·97	10·92	21·79	2·76	0·6	2·4	2·4	2·6	2·0
Er	18·25	18·19	41·57	73·47	11·18	2·3	9·2	10·4	9·7	9·3
Tm	3·93	4·28	6·97	12·52	2·30	0·7	2·0	2·4	2·4	1·9
Yb	33	39·32	54·64	91·11	19·29	7·5	16·5	18·9	19·0	18·0
Lu	7·54	8·97	10·67	17·29	4·75	2·2	3·8	4·3	4·5	4·2
Hf	2·28	1·97	3·68	11·46	3·05	1·5	2·6	3·4	3·4	1·8
Ta	0·94	0·8	0·62		0·58	1·1	1·7	1·3	1·7	1·0
Pb	10·04	15·45	18·09	38·45	30·93	23·4			14·5	22·8
Th	1·12	0·78	0·94	1·91		0·9		1·8	1·4	0·7
U	1·23	1·31	1·33	3·32	1·11	1·3		2·5	2·6	0·6

(continued)

Table 1: Continued

Sample:	OM94-78	OM94-80	OM94-99	OM94-110[1]	OM94-111[1]	OM94-112[1]
Lithology:	dunite	dunite	dunite	dunite	dunite	dunite
Mineralogy:	ol, sp	ol, sp	ol, sp	ol, sp	ol, sp	ol, sp
UTM E:	638436	639361	640230	640746	640914	640914
UTM N:	2546829	2546074	2539436	2533708	2533637	2533637
Depth below Moho (m):	4895	4910	2325	510	550	550
wt %						
SiO_2	35·60	35·74	35·50	37·79	36·33	37·71
TiO_2	0·007	0·011	0·012	0·012	0·018	0·016
Al_2O_3	0·34	0·20	0·14	0·25	0·48	1·91
FeO*	8·10	8·14	8·98	8·98	9·21	9·25
MnO	0·117	0·128	0·138	0·126	0·143	0·144
MgO	43·16	43·12	42·76	41·70	43·60	42·75
CaO	0·15	0·11	0·09	0·50	0·22	0·78
Na_2O	0·09	0·09	0·09	0·09	0·10	0·09
K_2O	0·00	0·00	0·00	0·00	0·00	0·00
P_2O_5	0·010	0·011	0·011	0·013	0·011	0·011
Cr_2O_3	0·421	0·419	0·446	0·351	0·626	0·430
LOI	11·05	11·53	11·60	9·81	9·53	7·52
Total	99·03	99·50	99·77	99·63	100·26	100·63
Mg-no.	90·48	90·43	89·46	89·22	89·41	89·17
ppm						
Li	0·36	0·60	0·40	0·64	0·60	1·90
Sc	3·8	4·9	4	4·6	4·4	4·5
Ti	11·9	31·3	42·6	40·7	76·4	61·3
Co	121	127	130	117	116	117
Ni	2636	2344	2451	2358	2195	2145
Cu	112·0	7·8	4·2	3·8	2·8	19·4
ppb						
Rb	4·5		30·4	26·0	14·4	12·9
Sr	30		148	35978	323	1329
Y	23·6		36·2	74·3	142·1	123·2
Zr	13·7		33·6	87·2	192·0	132·7
Nb	16·1		24·4	14·0	17·3	17·4
Cs	1·5			2·6	2·6	4·6
Ba	74			2119	55	82
La			0·6	7·9	10·6	12·1
Ce	1·7		2·5	15·8	19·0	25·8
Pr			0·7	2·0	3·4	4·5
Nd	5·1		4·6	7·3	19·0	24·4
Sm						8·9
Eu				1·8	3·2	10·5
Gd	3·0			5·7	12·5	13·4
Tb	0·5			1·1	2·8	2·2
Dy	4·8		5·8	11·1	21·8	18·5
Ho	1·3		1·8	3·2	6·3	5·2
Er	6·2		8·3	14·8	22·0	18·6
Tm	1·4		1·7	3·1	4·4	4·3
Yb	12·7		14·7	26·3	35·2	32·6
Lu	3·2		3·5	6·3	7·7	7·2
Hf	1·6			3·3	6·7	5·8
Ta	1·1		0·7	0·9	1·0	
Pb	39·1		17·1	25·1		
Th	1·0		1·3	2·5	1·1	1·0
U			1·5	16·2	2·2	2·1

(continued)

[1]Denotes re-enriched sample. (See text for details.)
*Total Fe given as FeO.
When samples have the same numbers ending with h or d, this denotes immediately adjacent samples of harzburgite and dunite, respectively. Generally, samples with higher numbers are higher in the section, so that samples with numbers above 100 are located close to the base of gabbroic crust. UTM (Universal Transverse Mercator coordinate system) coordinates are zone 40N.

UTM coordinates for each sample. Our sample transect is intersected by the Makhibiyah shear zone (Fig. 1), which is described as having no or little relative motion between the two adjacent blocks (Nicolas & Boudier, 2008). Harzburgites are coarse grained (1–5 mm) and have 10–15% orthopyroxene, ~5% spinel and ~85% olivine, which is about 50% serpentinized. Trace ($\ll$1%) amounts of clinopyroxene are found in one of the samples from this study, but may be present everywhere in very small abundances and perhaps not seen in thin section. Dunites are also coarse grained (1–5 mm) and consist of more than 90% olivine (about 50% serpentinized) and 5–10% spinel. Orthopyroxene has not been observed in any of the samples; clinopyroxene has been observed ($\ll$1%) in two samples and, as for the harzburgites, may be ubiquitous in trace amounts.

Whole-rock major elements and Ni, Sc, Ti, Co were analyzed by X-ray fluorescence (XRF) at the WSU Geoanalytical Laboratory; a description of the analytical procedures as well as analytical uncertainty has been given by Johnson *et al.* (1999). Trace elements were analyzed by inductively coupled plasma mass spectrometry (ICP-MS) at the University of Montpellier (see Godard *et al.*, 2000, for analytical details). Major and trace element analyses are given in Table 1.

Olivine, orthopyroxene, clinopyroxene and spinel were analyzed for their major element compositions by wavelength-dispersive spectrometry using a JEOL JXA-733 Superprobe at the Massachusetts Institute of

Technology. The accelerating voltage and beam current used were 15 kV and 10 nA, respectively. Typical counting times were 20–40 s and 1σ standard deviations of the counts were 0·5–1% (see Chatterjee *et al.*, 2005, for analytical details). Mineral analyses are given in Tables 2–5.

Os isotopic analyses were carried out at the University of Maryland using Carius tube digestion (Shirey & Walker, 1995) and negative thermal ionization mass spectrometry (N-TIMS), and at Woods Hole Oceanographic Institution (WHOI) using NiS flux fusion digestions

Table 2: Orthopyroxene analyses (sample numbers are prefixed OM94-)

Sample:	52h	53	61	67	74h	79	81	98	100	101	103	104	106	114	115
Lithology:	Harzb	Harzb	Harzb	Harzb	Harzb	Harzb	Harzb	Harzb	Harzb	Harzb	Harzb	Harzb	Harzb	Harzb	Harzb
wt %															
SiO_2	55·47	56·88	56·02	55·37	56·45	56·03	56·36	55·77	55·72	56·06	55·25	56·17	56·01	55·66	56·48
TiO_2	0·03	0·02	0·04	0·04	0·03	0·03	0·02	0·02	0·01	0·00	0·05	0·02	0·01	0·07	0·01
Al_2O_3	2·74	1·89	2·41	2·93	2·37	2·28	1·95	2·57	2·40	1·98	2·70	2·18	2·01	2·32	1·80
Cr_2O_3	0·71	0·58	0·70	0·61	0·55	0·51	0·60	0·77	0·74	0·60	0·90	0·75	0·73	0·81	0·74
FeO	6·02	5·86	5·41	6·02	6·03	6·27	6·19	6·16	6·12	6·35	5·87	6·00	5·81	6·18	5·78
MnO	0·14	0·14	0·12	0·13	0·13	0·14	0·13	0·13	0·13	0·14	0·13	0·14	0·14	0·15	0·13
MgO	33·74	34·44	34·34	33·80	33·83	33·96	34·11	33·70	33·47	33·54	31·39	32·98	34·14	32·46	33·19
CaO	0·92	0·67	0·74	0·67	0·67	0·49	0·64	0·84	0·98	1·16	3·08	1·90	1·30	2·45	2·48
Na_2O	0·00	0·00	0·00	0·00	0·00	0·00	0·00	0·01	0·00	0·00	0·19	0·01	0·02	0·01	0·03
Total	99·79	100·48	99·77	99·58	100·07	99·72	100·00	99·96	99·59	99·85	99·55	100·14	100·18	100·10	100·66
Molar															
Mg-no.	90·91	91·29	91·88	90·92	90·91	90·61	90·76	90·70	90·69	90·40	90·64	90·74	91·28	90·35	91·10
Wo	1·74	1·25	1·40	1·28	1·27	0·94	1·21	1·58	1·86	2·19	6·58	3·62	2·43	4·68	4·66
En	89·13	89·95	90·42	89·57	89·57	89·58	89·49	89·09	88·82	88·23	84·42	87·26	88·87	85·93	86·67
Fs	9·13	8·80	8·17	9·15	9·16	9·48	9·30	9·33	9·32	9·58	9·01	9·12	8·69	9·40	8·67
n	5	8	3	6	5	5	1	10	3	5	6	9	5	2	5

n, number of analyses.

Table 3: Olivine analyses (sample numbers are prefixed OM94-)

Sample:	52h	53	61	67	74h	79	81	98	100	101	103	104	106	114	115
Lithology:	Harzb	Harzb	Harzb	Harzb	Harzb	Harzb	Harzb	Harzb	Harzb	Harzb	Harzb	Harzb	Harzb	Harzb	Harzb
wt %															
SiO_2	40·14	40·70	40·48	40·17	40·52	40·32	40·08	40·14	40·20	40·22	40·37	40·44	40·54	40·51	40·54
TiO_2	0·00	0·00	0·00	0·00	0·00	0·00	0·00	0·01	0·01	0·00	0·01	0·00	0·00	0·01	0·00
Al_2O_3	0·02	0·01	0·01	0·01	0·04	0·02	0·02	0·01	0·01	0·02	0·01	0·01	0·01	0·01	0·03
Cr_2O_3	0·00	0·00	0·00	0·00	0·00	0·00	0·00	0·00	0·00	0·00	0·00	0·00	0·01	0·01	0·02
FeO	9·13	8·77	7·90	8·74	8·99	8·97	9·20	9·13	9·02	9·41	10·03	9·09	8·73	9·79	9·11
MnO	0·12	0·12	0·10	0·12	0·14	0·12	0·13	0·13	0·14	0·14	0·14	0·12	0·13	0·15	0·12
MgO	51·16	50·13	51·78	51·25	50·88	50·54	51·12	50·82	50·60	50·34	50·64	49·91	51·86	50·82	51·30
CaO	0·02	0·02	0·02	0·02	0·03	0·02	0·02	0·02	0·04	0·02	0·02	0·02	0·03	0·04	0·08
NiO	0·39	0·40	0·40	0·41	0·40	0·40	0·40	0·40	0·39	0·40	0·40	0·42	0·42	0·36	0·39
Total	100·99	100·14	100·69	100·73	101·00	100·39	100·96	100·67	100·41	100·54	101·62	100·00	101·72	101·68	101·61
Fo	90·90	91·06	92·12	91·26	90·98	90·94	90·83	90·84	90·91	90·51	90·00	90·73	91·37	90·25	90·93
n	3	8	3	3	3	3	3	7	3	3	5	4	2	2	3

(continued)

Table 3: Continued

Sample:	55	57	69	78	80	99	110	111	112
Lithology:	Dunite	Dunite	Dunite	Dunite	Dunite	Dunite	Dunite	Dunite	Dunite
wt %									
SiO_2	40·85	40·85	41·27	40·73	39·94	40·35	40·32	40·08	40·32
TiO_2	0·00	0·00	0·00	0·00	0·00	0·00	0·02	0·02	0·02
Al_2O_3	0·01	0·01	0·01	0·02	0·03	0·00	0·07	0·02	0·01
Cr_2O_3	0·00	0·00	0·00	0·00	0·00	0·00	0·02	0·02	0·01
FeO	8·73	8·75	7·93	9·15	9·05	9·86	9·15	9·72	9·94
MnO	0·12	0·13	0·13	0·16	0·15	0·15	0·14	0·15	0·15
MgO	49·16	49·70	50·71	50·23	51·16	48·79	49·44	49·37	49·08
CaO	0·06	0·07	0·19	0·07	0·06	0·09	0·20	0·14	0·12
NiO	0·38	0·36	0·40	0·36	0·35	0·34	0·34	0·33	0·32
Total	99·31	99·87	100·64	100·73	100·73	99·58	99·69	99·85	99·98
Fo	90·94	91·01	91·93	90·73	90·97	89·82	90·60	90·06	89·80
n	5	10	3	3	3	2	8	8	9

n, number of analyses.

(Ravizza & Pyle, 1997) followed by ICP-MS sparging (Hassler *et al.*, 2000). For Carius tube digestion, 1 g of sample powder was placed in a thick-walled borosilicate glass vessel. Reverse aqua regia (two parts concentrated HNO_3 and one part concentrated HCl) and a tracer solution enriched in ^{185}Re and ^{190}Os were added to the vessel, which was then sealed and held at 240°C for 3 days. The closed-system nature of this method ensures no volatile loss of Os, and the high temperatures and highly oxidizing nature of aqua regia ensure that the mixed Os and Re tracer equilibrates with the Os and Re in the sample. Re was extracted by anion exchange chemistry; Os was extracted by carbon tetrachloride solvent extraction, followed by stabilization in 9N HBr, and finally purified by microdistillation. Os was analyzed by N-TIMS, and Re by ICP-MS. Osmium was measured on Pt filaments using the MAT 262 thermal ionization mass spectrometer at the University of Maryland, with a typical precision (2σ) of <0·3% (Creaser *et al.*, 1991; Volkening *et al.*, 1991). Osmium and Re processing blanks are <3 pg and <10 pg, respectively (see Lee *et al.*, 2000, for complete analytical details). Ravizza & Pyle (1997) described the low-blank method for analyzing Os isotope ratios and complementary PGE concentrations on the same sample split using NiS fire assay, and a brief summary is given below. A mixed tracer enriched in ^{99}Ru, ^{105}Pd, ^{190}Os, ^{191}Ir, and ^{198}Pt is added to the sample prior to the NiS fire assay. After the fusion, the NiS bead is dissolved in 6·2N HCl and the remaining particulates are filtered through a 0·45 μm cellulose filter. The filter paper is dissolved in 1–2 ml concentrated HNO_3 and Os is oxidized to OsO at high temperature. After complete dissolution of the filter paper and oxidation of Os to OsO_4, the sample is chilled in ice water in a sealed beaker. The acidic solution is then diluted 10-fold with ultrapure water and analyzed by sparging it into a single-collector, magnetic sector ICP-MS system (Finnigan ELEMENT) at WHOI (see Hassler *et al.*, 2000, for a detailed description of the sparging method). Whole-rock PGE concentrations were determined by isotope dilution using the same NiS fusions as for the Os isotope composition analyses, and were analyzed by conventional ICP_MS using an APEX desolvating nebulizer on a single-collector ICP_MS (ThemoFisher Element2) at WHOI. Re was analyzed by isotope dilution (also by ICP-MS at WHOI) on a separate aliquot following an HF–HNO_3 acid digestion and ion exchange separation procedure (Reisberg *et al.*, 1991, 1993; Hauri & Hart, 1993). Estimated NiS fusion blanks are 1 pg (0.5 to 2 pg) Os and Ir and 20–30 pg Pd and Pt. Os data analyses, PGE and Re concentrations are given in Table 6.

Sulfur concentrations were measured at the University of Leicester (UK), by Saunders and coworkers, on a LECO CS 125 determinator. Samples along with iron and tungsten chip accelerants were loaded into a radio frequency induction furnace. The system was initially purged with oxygen, which then continued to stream throughout the combustion process. Power was applied until the accelerants were molten, and the sulfur was given off as SO_2. The combustion gases were then passed through a drying tube of magnesium perchlorate and then to the SO_2 IR cell. The IR absorption cells used a tungsten filament as the source, heated to ~850°C. The IR signal was then chopped at ~85 Hz and filtered to achieve a monochromatic IR wavelength corresponding to the energy of the SO_2 absorption wavelength. The output from the cells was monitored at 4 Hz, converted from an analogue signal to a digital signal, and the areas of the peaks were integrated. These values were then corrected for sample weight, blank value and calibration factors to give the final result. The calibration used geological reference materials and synthetic standards. The lower limit of detection for S is 10 ppm with a precision of ±8%.

RESULTS

Major and trace elements

The Wadi Tayin peridotites are generally as depleted in major and incompatible trace elements as the most depleted abyssal peridotites, or more depleted than them (Fig. 2). However, there are exceptions. Of the 16 harzburgites and 11 dunites analyzed for this study, three harzburgites and four dunites are relatively enriched in incompatible trace elements and are interpreted (see discussion below) as having been re-enriched, probably via igneous processes. Although intergranular plagioclase, whose presence in highly depleted peridotites is almost certainly due to partial crystallization of cooling melt

Table 4: Spinel analyses (sample numbers are prefixed OM94-)

Sample:	52h	53	61	67	79	81	74h	100	101	98	103
Lithology:	Harzb	Harzb	Harzb	Harzb	Harzb	Harzb	Harzb	Harzb	Harzb	Harzb	Harzb
wt %											
SiO_2	0·02	0·02	0·02	0·00	0·00	0·01	0·03	0·02	0·03	0·04	0·02
TiO_2	0·08	0·08	0·10	0·01	0·03	0·09	0·06	0·06	0·05	0·05	0·06
Al_2O_3	32·39	26·09	29·44	37·40	32·75	26·05	32·82	27·29	25·02	30·08	24·35
Cr_2O_3	36·27	43·09	40·05	30·62	33·92	41·83	35·28	40·78	43·28	38·18	43·19
FeO	14·88	17·02	14·42	14·37	16·58	17·80	15·11	17·46	17·72	16·31	18·97
Fe_2O_3	2·06	1·99	2·04	2·10	2·03	1·98	2·05	2·00	1·97	2·03	1·95
FeO*	16·73	18·81	16·25	16·26	18·41	19·58	16·96	19·26	19·49	18·13	20·72
MnO	0·22	0·27	0·23	0·15	0·19	0·26	0·21	0·27	0·30	0·22	0·28
MgO	14·63	12·71	14·48	15·55	14·19	12·76	14·50	13·22	12·35	13·78	11·77
CaO	0·01	0·01	0·01	0·00	0·01	0·00	0·01	0·01	0·01	0·00	0·00
NiO	0·14	0·09	0·12	0·12	0·10	0·06	0·12	0·09	0·08	0·12	0·10
Total	100·69	101·37	100·91	100·32	99·80	100·85	100·19	101·20	100·80	100·81	100·68
Molar											
Cr-no.	42·89	52·57	47·73	35·46	41·00	51·85	41·90	50·06	53·72	46·00	54·34
Mg-no.	63·80	57·26	64·29	65·99	60·53	56·25	63·23	57·57	55·54	60·22	52·66
n	3	8	3	3	3	3	3	3	3	7	5

Sample:	104	106	114	115	55	69	78	80	99
Lithology:	Harzb	Harzb	Harzb	Harzb	Dunite	Dunite	Dunite	Dunite	Dunite
wt %									
SiO_2	0·00	0·21	0·04	0·03	0·00	0·00	0·03	0·01	0·00
TiO_2	0·03	0·03	0·28	0·04	0·05	0·22	0·30	0·35	0·45
Al_2O_3	24·55	22·75	24·69	21·10	30·51	20·91	20·52	17·17	12·10
Cr_2O_3	43·46	43·58	42·15	48·03	37·36	45·33	41·59	46·49	49·67
FeO	17·92	16·28	18·67	17·13	15·45	19·38	24·36	25·26	26·63
Fe_2O_3	1·96	1·91	1·95	1·95	3·51	1·94	1·88	1·84	1·78
FeO*	19·68	18·00	20·43	18·88	18·61	21·12	26·06	26·92	28·24
MnO	0·26	0·27	0·27	0·28	0·22	0·27	0·33	0·39	0·38
MgO	12·35	12·64	12·00	12·53	14·05	13·09	11·24	8·85	8·99
CaO	0·00	0·01	0·02	0·00	0·00	0·00	0·01	0·00	0·00
NiO	0·08	0·07	0·11	0·10	0·12	0·13	0·17	0·08	0·11
Total	100·62	97·76	100·19	101·18	101·28	101·27	100·44	100·43	100·12
Molar									
Cr-no.	54·29	56·33	53·39	60·43	45·10	59·25	57·62	64·48	73·35
Mg-no.	55·27	58·22	53·51	56·75	62·07	54·78	45·30	38·59	37·71
n	4	2	2	3	5	3	3	3	2

n, number of analyses.

migrating along grain boundaries in a depleted residue, is sometimes reported in Oman peridotites the samples in this study show no macroscopic evidence for enrichment or impregnation. The re-enriched samples are clearly distinguished on a plot of chondrite normalized [denoted (N)] Ce/Yb against Al_2O_3 (Fig. 2e). Most of the Wadi Tayin samples have low Ce/Yb (N) compared with abyssal peridotites. The re-enriched samples have elevated Ce/Yb (N) and/or Al_2O_3. These re-enriched samples are shown using blue symbols in this and subsequent figures

Table 5: Clinopyroxene analyses (sample numbers are prefixed OM94-)

Sample no.:	81	57	69
Lithology:	Harzb	Dunite	Dunite
wt %			
SiO_2	53·43	54·33	53·72
TiO_2	0·08	0·10	0·10
Al_2O_3	2·09	1·42	2·34
Cr_2O_3	0·81	0·59	0·96
FeO	1·99	1·57	1·69
MnO	0·07	0·03	0·02
MgO	17·60	17·45	17·06
CaO	24·37	25·44	25·10
Na_2O	0·15	0·07	0·24
Total	100·60	100·99	101·24
Molar			
Mg-no.	94·04	95·19	94·75
Wo	48·29	49·92	50·04
En	48·52	47·63	47·30
Fs	3·19	2·45	2·66
n	3	2	4

n, number of analyses.

(harzburgites 103, 114 and 115, and dunites 52d, 110, 111 and 112). All but one of these samples are shallow-level peridotites, structurally from less than 550 m below the crust–mantle transition. The exception is 52d, a deep dunite that is anomalously rich in Al, Cr, Ti and Sr, though not Ca. The samples are typically 30–50% serpentinized, and there is no correlation between serpentinization [as observed in thin section and as reflected by loss on ignition (LOI), Table 1] and major and trace element abundances or ratios.

Harzburgites have MgO and FeO contents similar to those of many depleted abyssal peridotites (Fig. 2a and b), but tend to have low Al_2O_3, SiO_2 and CaO (Fig. 2c–e) and incompatible trace element abundances as exemplified by Ce/Yb and Ti in Fig. 2e and f. Dunites have higher MgO and FeO* contents and lower SiO_2, Al_2O_3 and CaO than harzburgites, reflecting their higher olivine contents. In addition, dunites tend to be more completely serpentinized than harzburgites; thus, some of the chemical differences between dunites and harzburgites could be produced or enhanced by alteration. Molar Mg-numbers [$100 \times$ Mg-number $=$ MgO/(MgO + FeO)] are between 89·2 and 91·8 for both harzburgites and dunites. The compositions of, and differences between harzburgites and dunites are similar to those reported by Godard *et al.* (2000) and Monnier *et al.* (2006).

Table 6: Platinum group elements (PGE) and Os isotopic composition

Sample:	52h	52h	53	54	61	67	79	79	81	74h	74h
Lithology:	Harzb	Harzb	Harzb	Harzb	Harzb	Harzb	Harzb	Harz	Harzb	Harzb	Harzb
PGE (ppt)											
Os	3898	3840	4658	4788	4583	4114	5066		4795	4212	4266
Ir	3789	4086	4539	4324	4175	4117	4889		4054	3726	3624
Ru	7863	7357	9065	8946	7769	11172	10200		9753	8746	9758
Pt	9359	7830	8879	23888	5060	9261	12730		11232	8959	8447
Pd	11729	11892	13980	19074	11956	6664	10021		11046	8378	16891
Ir/Os	0·9721	1·0640	0·9744	0·9031	0·9109	1·0007	0·9652		0·8454	0·8846	0·8496
Os (ppt)*	3903	4179	4799	4773	3640	4314	4601	4612	4659	3983	4508
Re (ppt)	826·4		831·5	553·7	123·8	407·8		289·8	648·9	759·4	
$^{187}Re/^{188}Os$	1·02		0·84	0·56	0·16	0·46		0·30	0·67	0·92	
$^{187}Os/^{188}Os$	0·1249	0·1257	0·1241	0·1286	0·1162†	0·1235	0·1246	0·1245†	0·1315	0·1264	0·1267
2σ	0·0005	0·001	0·0006	0·001	0·00002	0·0007	0·0005	0·0055	0·001	0·001	0·001
$^{187}Os/^{188}Os$ (t^{90})	0·1233	0·1241	0·1228	0·1277	0·1159	0·1228	0·1241	0·1241	0·1305	0·1250	0·1253
S (ppm)	29·67		56·00	33·00	18·67	18·67	23·33		29·00	29·00	
Cu (ppm)	8·9		18	24·1	8·4	11·2	17·5		26·5	18·7	
Cu/S	0·3000		0·3214	0·7303	0·4500	0·6000	0·7500		0·9138	0·6448	

(continued)

Table 6: Continued

Sample:	100	101	98	98	103	103	104	106	114	114	114	115
Lithology:	Harzb	Harzb	Harzb			Harzb	Harzb	Harzb	Harzb	Harzb	Harzb	Harzb
PGE (ppt)												
Os	4510	4966	6367			5177	4648	4686	3698	4406		4851
Ir	3857	4251	4362			4753	4022	4186	5236	5732		4099
Ru	8872	8506	9114			8933	8619	9106	8089	7620		8477
Pt	10621	9843	10532			11001	9693	10408	8118	7685		11934
Pd	2029	14033	11552			22533	14095	14535	1583	1557		11526
Ir/Os	0·8552	0·8561	0·6851			0·9181	0·8652	0·8934	1·4162	1·3009		0·8449
Os (ppt)*	4666	5076	3850	5381	5246	4780	4702	2840	4180	4612	3880	5249
Re (ppt)	772·6	732·5	217·4			434·5	3703	221·2	355·6			690·7
$^{187}Re/^{188}Os$	0·80	0·70	0·27			0·44	3·80	0·38	0·27			0·63
$^{187}Os/^{188}Os$	0·1251	0·1304	0·1244†	0·1244	0·1323	0·1312†	0·1294	0·1368	0·1225	0·1234	0·1227	0·1302
2σ	0·0006	0·0005	0·00002	0·0004	0·0010	0·00004	0·0008	0·00005	0·00002	0·001	0·0013	0·0014
$^{187}Os/^{188}Os$ (t^{90})	0·1239	0·1293	0·1240	0·1240	0·1316	0·1305	0·1235	0·1362	0·1220	0·1230	0·1223	0·1292
S (ppm)	28·00	5·67	41·00			100·00	20·00	11·50	23·67			24·33
Cu (ppm)	7·7	17·7	11			28·3	17	11·1	15·9			9·4
Cu/S	0·2750	3·1235	0·2683			0·2830	0·8500	0·9652	0·6718			0·3863

Sample:	115	52d	52d	52d	55	55	57	57	69	69	69	69	78	78
Lithology:	Harzb	Dunite	Dunite		Dunite	Dunite	Dunite	Dunite	Dunite	Dunite	Dunite	Dunite	Dunite	Dunite
PGE (ppt)														
Os	4624	859	787		2046	1858	5141	4592	2748	2718	2852	2790	4986	5030
Ir	4066	1208	1214		3673	4032	7169	7129	1625	1636	554		4762	4790
Ru	8555	2489	2341			4413	9363	8932	6719	6387	7303	7219	13105	13063
Pt	11712	4363	4540		7663	9321	22378	20467	1333	1359	1996	2059	34655	31545
Pd	11266	4642	4470		10275	14058	8154	7981	2804	2766	5734	5635	36641	
Ir/Os	0·8793	1·4064	1·5418		1·7956	2·1702	1·3944	1·5525	0·5913	0·6018	0·1941		0·9552	0·9524
Os (ppt)*		1860	910	1280	2450	1991	3910	4901	2830		2892		4380	5111
Re (ppt)		86			211		23		339·7				1410	
$^{187}Re/^{188}Os$		0·22			0·60		0·03		0·58				1·57	
$^{187}Os/^{188}Os$		0·1337†	0·1363	0·1381	0·1239†	0·1260	0·1268†	0·1270	0·1254		0·1253		0·1502†	0·1528
2σ		0·00002	0·0013	0·0031	0·00004	0·0012	0·00004	0·0007	0·0007		0·0007		0·00003	0·0010
$^{187}Os/^{188}Os$ (t^{90})		0·1333	0·1360	0·1378	0·1229	0·1251	0·1268	0·1270	0·1245		0·1244		0·1477	0·1508
S (ppm)		39·00			31·67		34·33		13·67				56·33	
Cu (ppm)		8·4			1·4		3·6		2·5				84·3	
Cu/S		0·2154			0·0442		0·1049		0·1829				1·4964	

(continued)

MORB-normalized whole-rock trace element abundances are plotted in Fig. 3. Overall, the Wadi Tayin peridotites are characterized by having slightly U-shaped patterns reflecting relative enrichment of the most incompatible elements relative to the light rare earth elements (LREE). Similar patterns were described by Godard *et al.* (2000) and Monnier *et al.* (2006) for other harzburgite and dunite samples from the southern part of the Oman ophiolite, and U-shaped patterns are also common in peridotites from other areas (e.g. Parkinson & Pearce, 1998; Bodinier & Godard, 2003; Niu, 2004; Paulick *et al.*, 2006). Apart from the overall U-shaped patterns, there are some notable features demonstrated in Fig. 3. (1) Across the entire incompatible element spectrum, the Oman peridotite samples

Table 6: Continued

Sample:	78	80	74d	74d	99	110	110	111	111	112	112
Lithology:	Dunite	Dunite	Dunite	Dunite	Dunite	Dunite	Dunite	Dunite	Dunite	Dunite	Dunite
PGE (ppt)											
Os	4919	3492	5096	5029	2177	4332	4122	3993	2173	3936	3993
Ir	4736	5140	1983	1951	3284	520	519	2209	2230	2419	2453
Ru	14467	8331	10054	11376	3323	7171	7176	5204	4933	5388	4977
Pt	35124	6352	19556	20076	15768	3474	3553	11817	11934	25999	29156
Pd	36953	9473		39490		8713	8657	8541	8528	35070	
Ir/Os	0·9629	1·4720	0·3890	0·3880	1·5090	0·1200	0·1260		1·0265	0·6147	0·6144
Os (ppt)*	5217	3435		5237	2197	4439			2200	4001	
Re (ppt)		610·2	528·6		247	420·2		210·2		368	
$^{187}Re/^{188}Os$		0·86	0·49		0·54	0·46		0·46		0·44	
$^{187}Os/^{188}Os$	0·1509	0·1298		0·1291	0·1269	0·1292		0·1321	0·1315†	0·1331	
2σ	0·0012	0·0011		0·0007	0·0009	0·001		0·0010	0·00003	0·0009	
$^{187}Os/^{188}Os$ (t^{90})	0·1485	0·1285		0·1283	0·1261	0·1285		0·1314	0·1308	0·1324	
S (ppm)		45·00		20·67	8·67	12·67			8·67	50·00	
Cu (ppm)		7·8		27·5	4·2	3·9			2·8	19·4	
Cu/S		0·1733		1·3306	0·4846	0·3079			0·3231	0·3880	

Samples listed more than once are re-runs of the sample for PGE, Os isotopic composition or both. t^{90} denotes age corrected to 90 Ma.
*Os concentration measured on isotope run.
†Analyses by N-TIMS.

have trace element concentrations at and below the lower limit for mid-ocean ridge peridotite data in the literature (Niu, 2004; Paulick *et al.*, 2006). (2) Unlike most mid-ocean ridge peridotites, the Oman samples have low middle to heavy REE (MREE/HREE) ratios, most probably reflecting fractionation of MREE from HREE during melting beyond the exhaustion of clinopyroxene. (3) All samples have a pronounced Pb enrichment relative to Ce and Nd and a small U enrichment relative to Th. (4) All but two harzburgites and all re-enriched samples have a pronounced Sr enrichment relative to Nd, whereas dunites that are not re-enriched either do not have Sr enrichment or have much less pronounced enrichment.

Overall, dunites have similar or lower abundances of highly incompatible elements compared with harzburgites, and lower abundances of the moderately incompatible elements. This is also seen in Fig. 4 for chondrite-normalized REE abundances. Harzburgites have consistently steeper REE patterns, with higher HREE concentrations and similar LREE concentrations compared with dunites. The seven re-enriched samples generally have elevated LREE abundances and are LREE enriched compared with the rest of the samples. As noted above, of the seven re-enriched samples, six are from a high stratigraphic level, less than 550 m below the crust–mantle transition. The exception, dunite sample 52d, which is the deepest of all the samples from ~10·5 km below the crust–mantle transition, has a spoon-shaped REE pattern (and very low abundances) and a markedly jagged trace element abundance pattern in Fig. 3, suggesting a different origin from the other re-enriched samples.

Mineral compositions are given in Tables 2–5. Olivine molar Mg-number [Forsterite content $= 100 \times MgO/(MgO + FeO)$] is similar in dunites and harzburgites (average of 90·9 for both groups) and slightly higher than the whole-rock Mg-number. Molar Cr-numbers [Cr-number $= 100 \times Cr_2O_3/(Cr_2O_3 + Al_2O_3)$] in spinel range from 35 to 73 and are on average higher in the dunites (average of ~60 for dunites and ~50 for harzburgites; Fig. 5). With just a few exceptions, the Wadi Tayin samples presented here plot within the array formed by mid-ocean ridge peridotite samples (Dick & Bullen, 1984; Arai, 1994) towards the more depleted end, as do most of our data on spinels in harzburgite from the NE corner of the nearby Samail massif (Braun, 2004). The exceptions in the Wadi Tayin data, with higher Cr-number than in mid-ocean ridge peridotites, are mainly spinels in dunites, and are similar to our extensive data on spinel in dunites in the Samail massif (Braun, 2004). These have spinel Cr-number between 65 and 75, higher than in abyssal peridotites but lower than many samples from the northern massifs of the Oman ophiolite. However, it should be noted that this comparison with mid-ocean ridge samples is flawed because of the paucity of data on spinels in

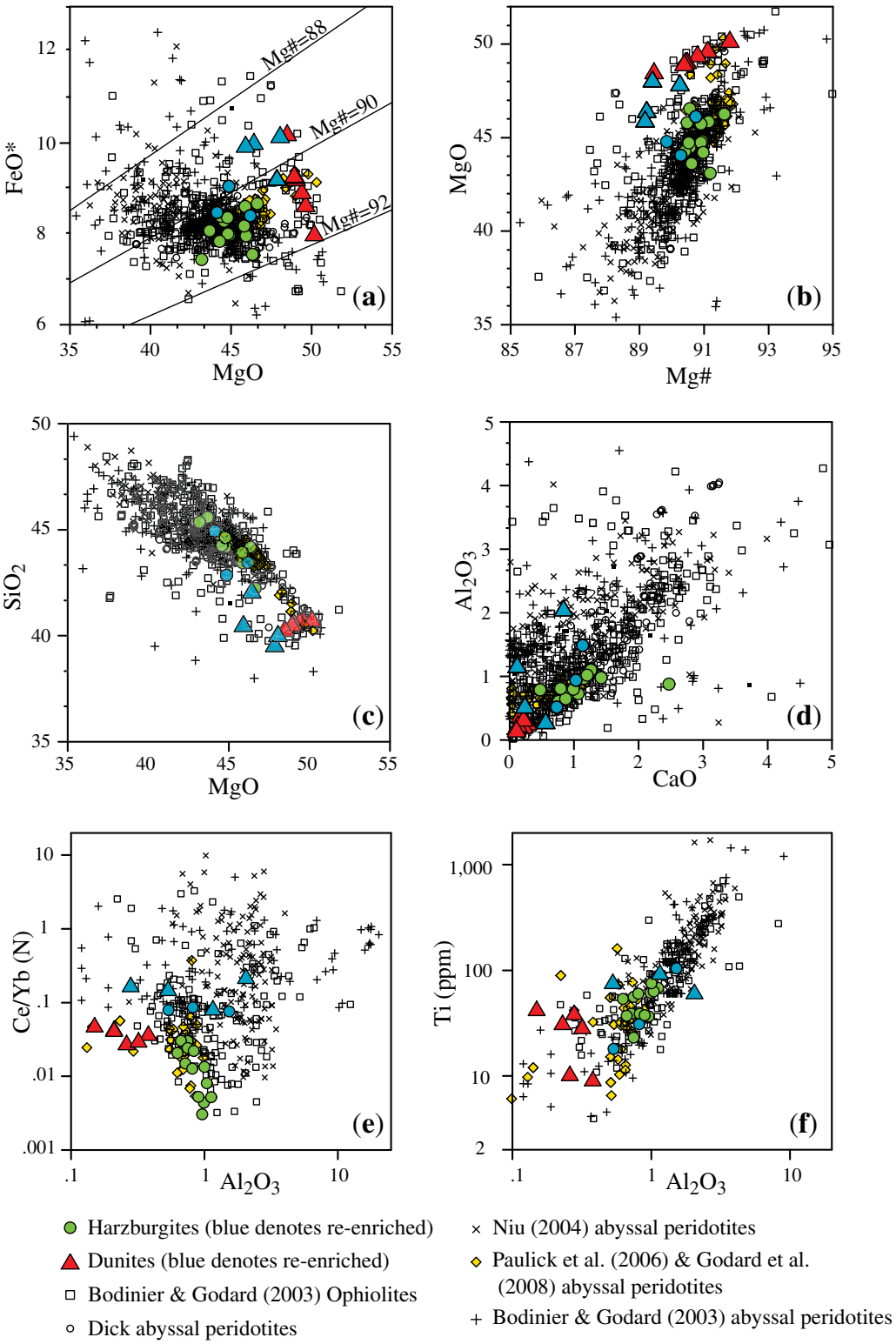

Fig. 2. Plots showing selected major and trace element variations in Wadi Tayin harzburgites and dunites compared with orogenic peridotites, abyssal peridotites and ophiolites. Data are normalized to 100% volatile-free and are from Dick (1989, and unpublished data), Bodinier & Godard (2003), Niu (2004), Paulick *et al.* (2006) and Godard *et al.* (2008). The data from Dick (1989, and unpublished data) are calculated whole-rock compositions from mineral analyses, all other data are XRF and ICP-MS on whole-rock. Red triangles indicate dunites; green circles, harzburgites; blue triangles and circles, re-fertilized dunites and harzburgites, respectively.

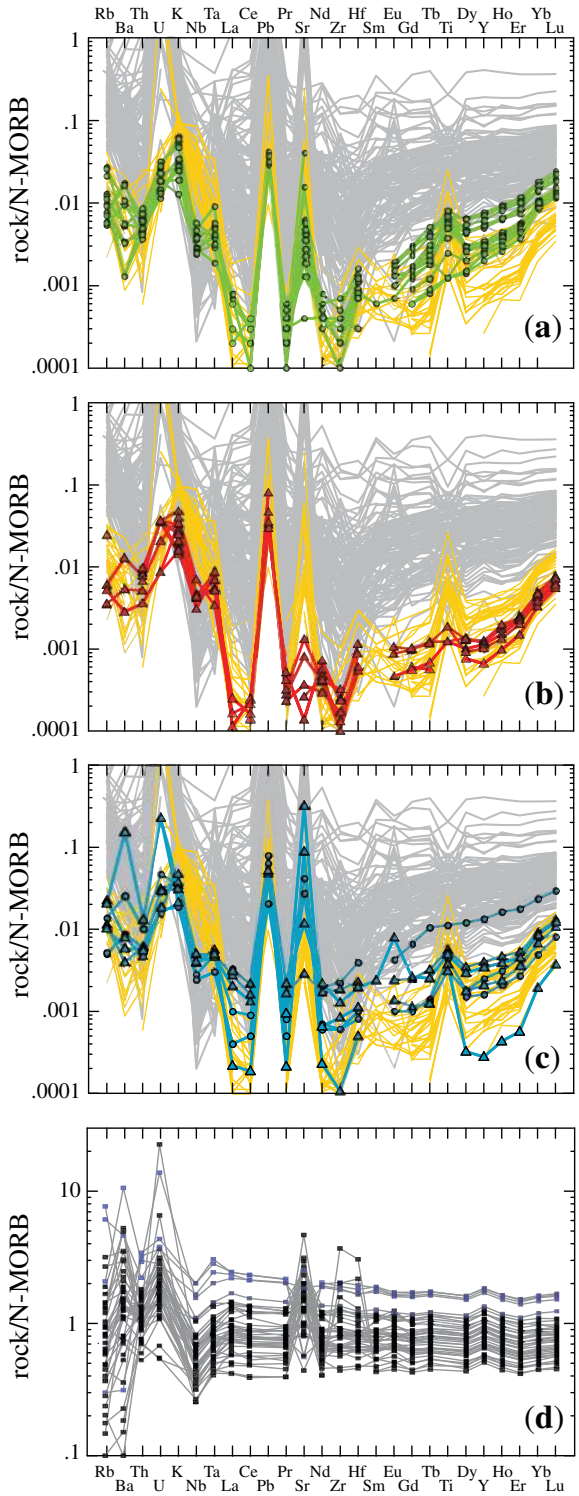

Fig. 3. MORB-normalized trace element abundance patterns (Hofmann, 1988); (a) harzburgites, (b) dunites, (c) re-fertilized or impregnated samples, (d) lavas (blue squares) and dikes (black squares) from the Samail and Wadi Tayin massifs of the Oman ophiolite (J. A. Pearce 2005, pesonal communication). Symbols as in Fig. 2. Abyssal peridotites are shown in (a)–(c) in light gray (Niu, 2004) and yellow (Paulick *et al.*, 2006).

mid-ocean ridge dunites. Dunites exposed on the seafloor at mid-ocean ridges are generally very heavily weathered and thus are commonly destroyed during dredging. Those dunites that are recovered are often too altered to recover primary spinel compositions. It could be that Cr-numbers in dunite spinels from mid-ocean ridges are higher than in corresponding residual peridotites from ridges, as in our Wadi Tayin and Samail datasets.

Orthopyroxenes in the harzburgites range from compositions similar to those in abyssal peridotites (H. J. B. Dick, 2007, pesonal communication; Dick, 1989) to compositions with lower CaO and Al_2O_3 and higher Mg-number (Fig. 6). Generally, harzburgites are somewhat less refractory in the upper part of the section compared with the lower part; that is, they have lower whole-rock Mg-number and higher whole-rock CaO and Al_2O_3, higher Na_2O in orthopyroxene and lower Mg-number in olivine (Figs 6 and 7).

In addition to these geochemical differences, mineral exchange thermometry yields higher temperatures for the uppermost mantle samples, compared with those deeper in the section. The generally high CaO contents of the orthopyroxene result in relatively high calculated temperatures using the Ca-in-orthopyroxene two-pyroxene solvus thermometer (Brey & Kohler, 1990; Figs 6 and 7). Because discrete crystals of clinopyroxene are rare in these rocks, the use of the two-pyroxene solvus and Ca in olivine–clinopyroxene thermometer could be problematic. For example, orthopyroxene undersaturated in clinopyroxene, as a result of extensive melting after the exhaustion of residual clinopyroxene, has low Ca contents that could yield spuriously low temperature estimates (Dick, 1977). However, orthopyroxene crystals in the Oman harzburgites always include extensive clinopyroxene exsolution lamellae, and thus were clinopyroxene saturated over much of their cooling path. The overall temperature range calculated from Ca-in-orthopyroxene is 800–1400°C. Temperatures calculated from other thermometers are lower (Figs 6 and 7), as expected when comparing closure temperatures for net transfer reactions (pyroxene solvus) with temperatures for cation exchange reactions (Fe–Mg, Ca–Mg and Cr–Al exchange between olivine, orthopyroxene, clinopyroxene, and spinel). Correlation of the Ca-in-opx solvus and Ca in olivine–clinopyroxene exchange temperatures with temperatures from other thermometers suggests that all record closure temperatures along the same cooling path for each sample, which reinforces the hypothesis that the pyroxene solvus and Ca in olivine–clinopyroxene thermometry is valid.

Os isotopes and PGE concentrations

Osmium isotopic compositions, PGE concentrations and sulfur concentrations are given in Table 6. In terms of $^{187}Os/^{188}Os$, both harzburgites and dunites are within the range of abyssal peridotite compositions (Fig. 8), but

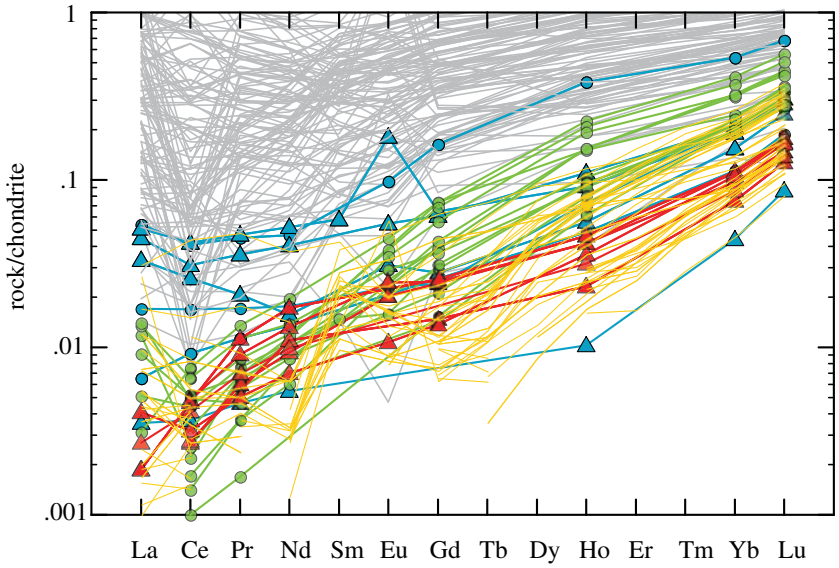

Fig. 4. Chondrite-normalized REE abundance patterns (Sun & McDonough, 1989). Symbols as in Fig. 3.

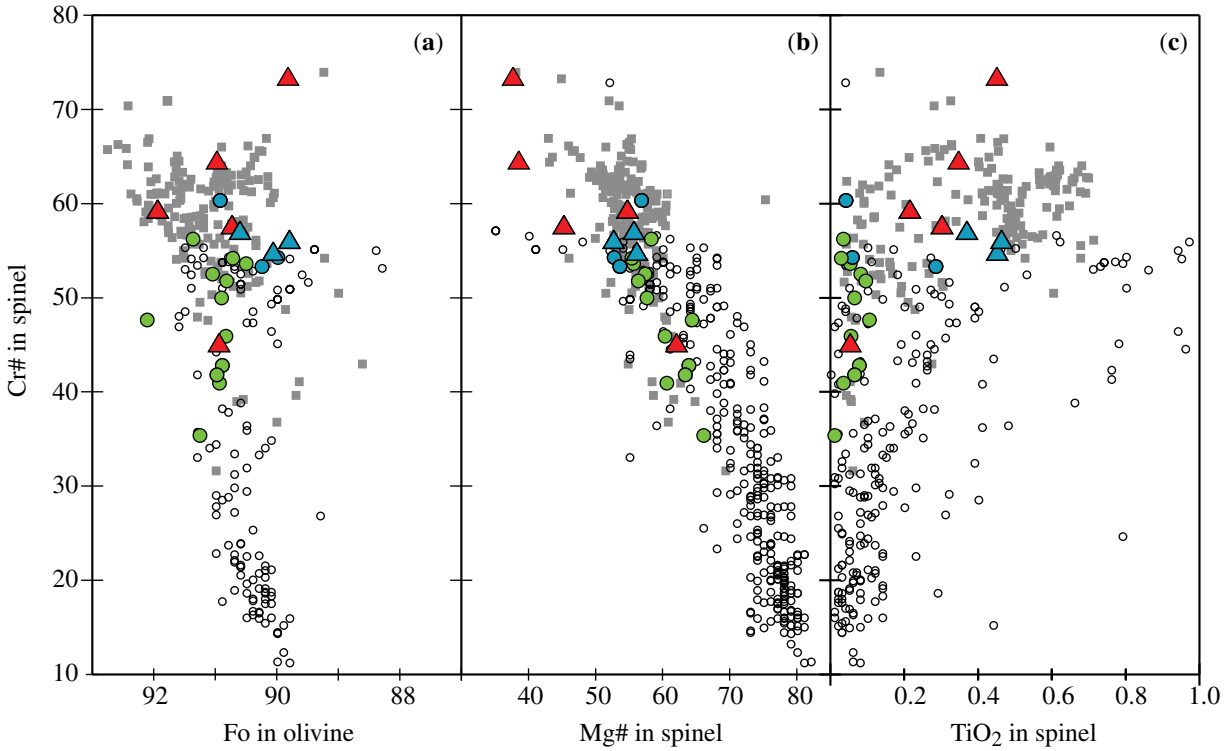

Fig. 5. Cr-number [100 × molar Cr/(Cr + Al)] in spinel vs (a) Fo content [100 × molar Mg/(Mg + Fe)] in coexisting olivine, (b) Mg-number [100 × molar Mg/(Mg + Fe)] in spinel, and (c) TiO_2 in spinel. Small grey squares are data from the Samail massif (Braun, 2004). Other symbols as in Fig. 2.

dunites, on average, have higher $^{187}Os/^{188}Os$, similar to MORB. Assuming that Re/Os and/or $^{187}Os/^{188}Os$ have not been modified by alteration processes postdating emplacement of the ophiolite, initial (at 90 Ma) $^{187}Os/^{188}Os$ compositions of harzburgites range from 0·1159 to 0·1362 (average = 0·1257), and of dunites from 0·1245 to 0·1477 (average = 0·1307). The Os isotopic compositions are similar to those reported by

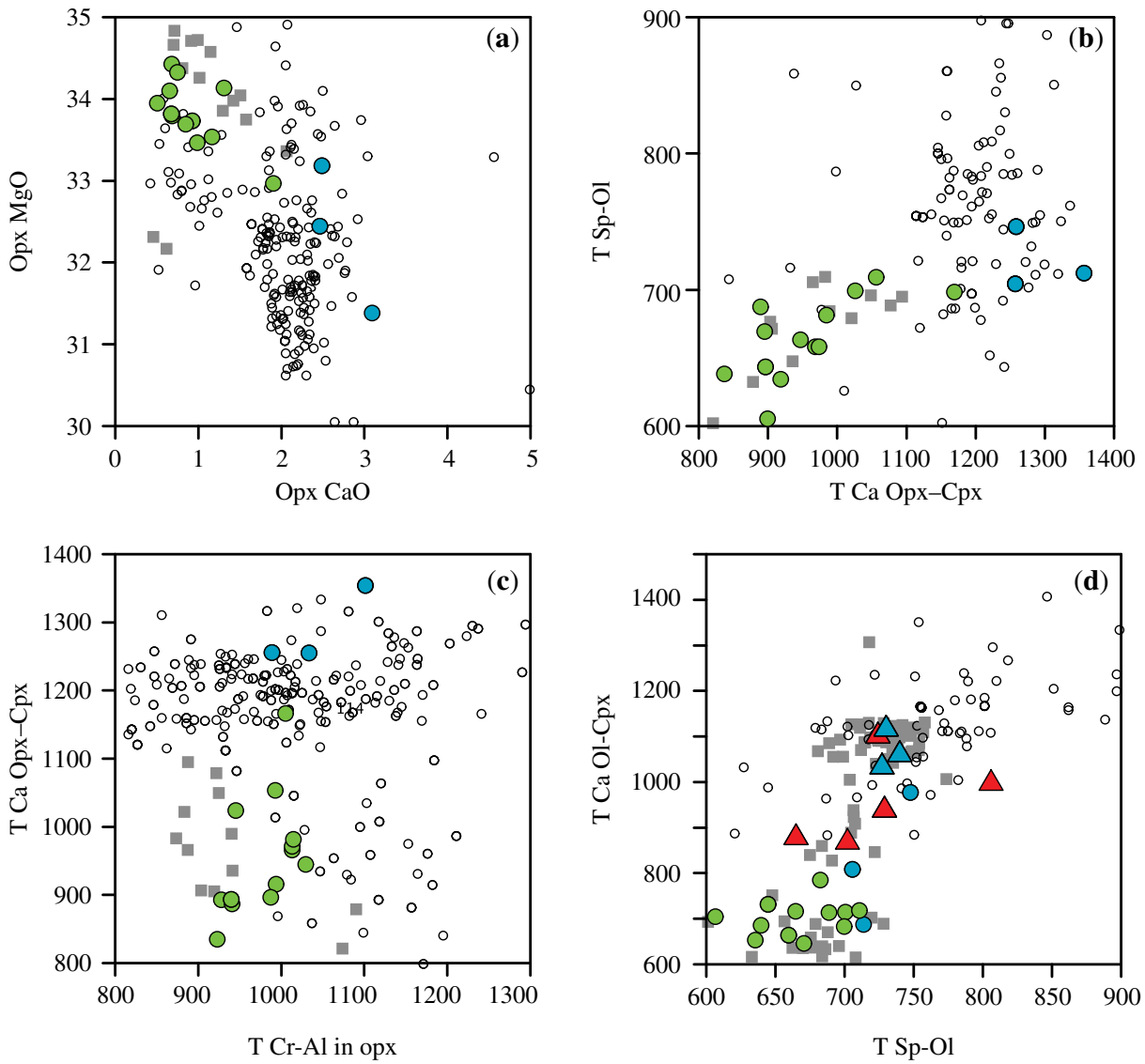

Fig. 6. Mineral chemistry and geothermometry. (a) MgO vs CaO in orthopyroxene; (b) temperature (T) calculated using Cr exchange between spinel and olivine (Sack & Ghiorso, 1991) vs T calculated using Ca exchange between opx and cpx (Brey & Kohler, 1990); (c) T calculated using Ca exchange between opx and cpx (Brey & Kohler, 1990) vs T calculated using Cr–Al exchange in opx (Witt-Eickschen & Seck, 1991); (d) T calculated using Ca exchange between olivine and clinopyroxene (Kohler & Brey, 1990) vs T calculated using Cr exchange between spinel and olivine (Sack & Ghiorso, 1991). For the thermometer utilizing Ca exchange between olivine and clinopyroxene, it is assumed that olivine in all rocks is in equilibrium with clinopyroxene, although clinopyroxene has only been found in three of the samples. For all harzburgites T is calculated using the clinopyroxene composition from OM94-81, and for all dunites T is calculated using the clinopyroxene composition from OM94-69. Small grey squares are peridotites in the Samail Massif (Braun, 2004).

Ahmed *et al.* (2006) for chromitites from the Oman ophiolite. There is no systematic relationship between 're-enrichment' in incompatible trace elements and $^{187}Os/^{188}Os$; instead, re-enriched samples have isotope ratios in the middle of the range for all samples. There is no correlation between Os isotopic composition and depth (not shown).

Harzburgites have flat PGE patterns and remarkably constant concentrations, except for the platinum and palladium concentrations, which vary by an order of magnitude (Fig. 9). In dunites, PGE abundances are generally lower and more variable than in harzburgites. This difference is reflected in the Os/Ir ratios. Harzburgites have Os/Ir ratios clustering tightly around unity, whereas Os/Ir in dunite ranges from 0·5 to 8·3 (Fig. 10). Os/Ir ratios do not correlate with isotopic composition, abundance of any of the other PGE elements, sulfur concentration, sample depth, or loss on ignition.

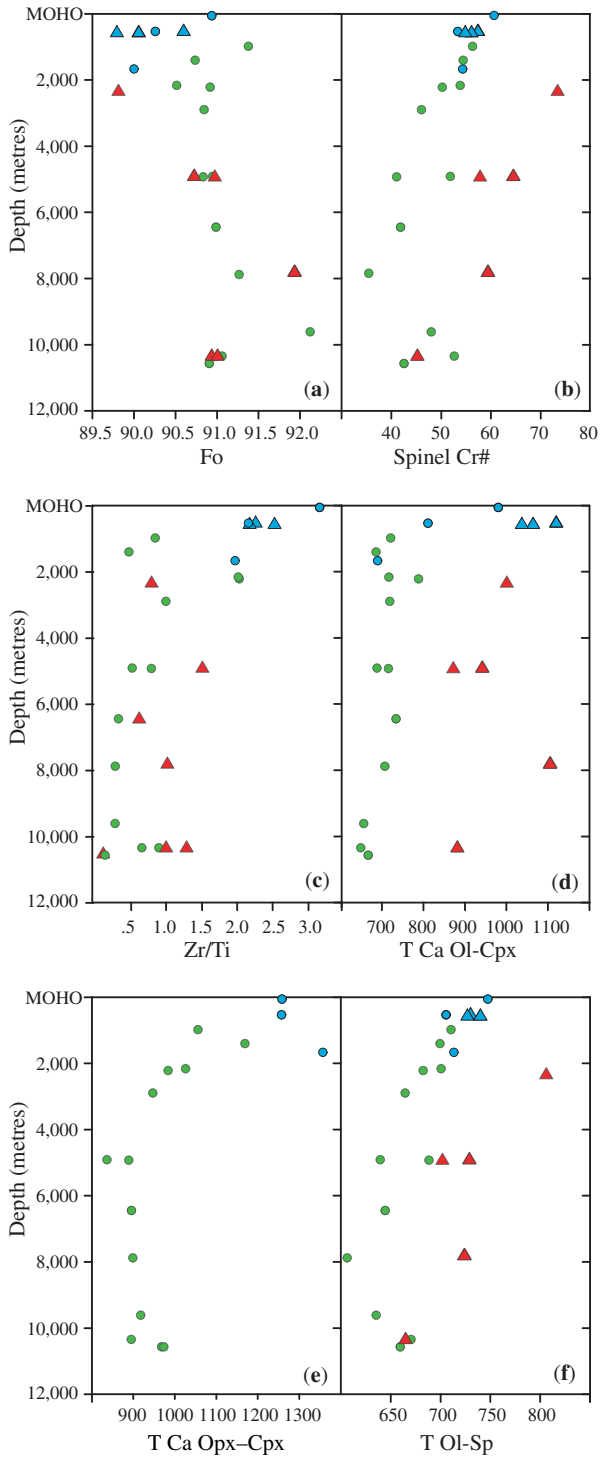

Fig. 7. Depth below the Moho Transition Zone vs (a) forsterite [100 × molar Mg/(Mg + Fe)] in olivine; (b) Cr-number [100 × molar Cr/(Cr + Al)] in spinel; (c) Zr/Ti in whole-rock; (d)–(f) *T* calculated using the thermometers listed in the caption for Fig. 6. Symbols as in Fig. 2.

DISCUSSION

Highly depleted residues

The Wadi Tayin harzburgites are residues of partial melting that are as depleted as the most depleted mid-ocean ridge peridotites (H. J. B. Dick, personal communication; Dick, 1989; Johnson *et al.*, 1990; Johnson & Dick, 1992; Dick & Natland, 1996; Niu, 1997, 2004; Bodinier & Godard, 2003; Harvey *et al.*, 2006; Paulick *et al.*, 2006; Godard *et al.*, 2008). Across the entire incompatible element spectrum, the Oman peridotite samples have trace element concentrations at and below the lower limit for mid-ocean ridge peridotites. Unlike most mid-ocean ridge peridotites, the Oman samples have low MREE to HREE ratios, most probably reflecting melting close to and beyond the exhaustion of clinopyroxene. Spinel Cr-numbers in the Oman harzburgites generally lie within the high end of the field defined by spinels from mid-ocean ridge peridotites; some spinel Cr-numbers in Oman dunites are higher than those in mid-ocean ridge dunites, although there are very few data on mid-ocean ridge dunites. Our data are consistent with previous work on Samail and Wadi Tayin peridotite compositions (Godard *et al.*, 2000; Monnier *et al.*, 2006), and our conclusions are enhanced by the availability of comparable data for whole-rock compositions of mid-ocean ridge peridotites (Niu, 2004; Paulick *et al.*, 2006).

The conclusion that Wadi Tayin harzburgites are residues of higher degrees of melt extraction from a fertile mantle source, compared with typical mid-ocean ridge peridotites, raises several questions. (1) Did partial melting beneath the Oman spreading ridge take place at unusually high temperature? (2) Or, was the H_2O content of the mantle source beneath the Oman spreading ridge unusually high? (3) Alternatively, was the Wadi Tayin mantle source depleted by previous melt extraction, prior to the partial melting beneath the Oman spreading ridge? Klein & Langmuir (1987) and Langmuir *et al.* (1992) have previously suggested that crustal thickness in mid-ocean ridge and ophiolite sections is inversely correlated with Na_2O concentration in clinopyroxene in primitive, crustal gabbros, relating thick crust to high degrees of melting—and Na_2O depletion—in the mantle source. Humler *et al.* (1999) showed that data from the Oman ophiolite lie at the high crustal thickness, low clinopyroxene Na_2O content end of the spectrum, which suggests that options (1) and/or (2) are more likely than (3) in this case.

Enrichment in highly incompatible elements: caused by grain boundary partitioning?

The U-shaped MORB-normalized trace element patterns, common in these and other peridotites, have been explained in various ways by different researchers. Prinzhofer & Allègre (1985), Kelemen (1986) and

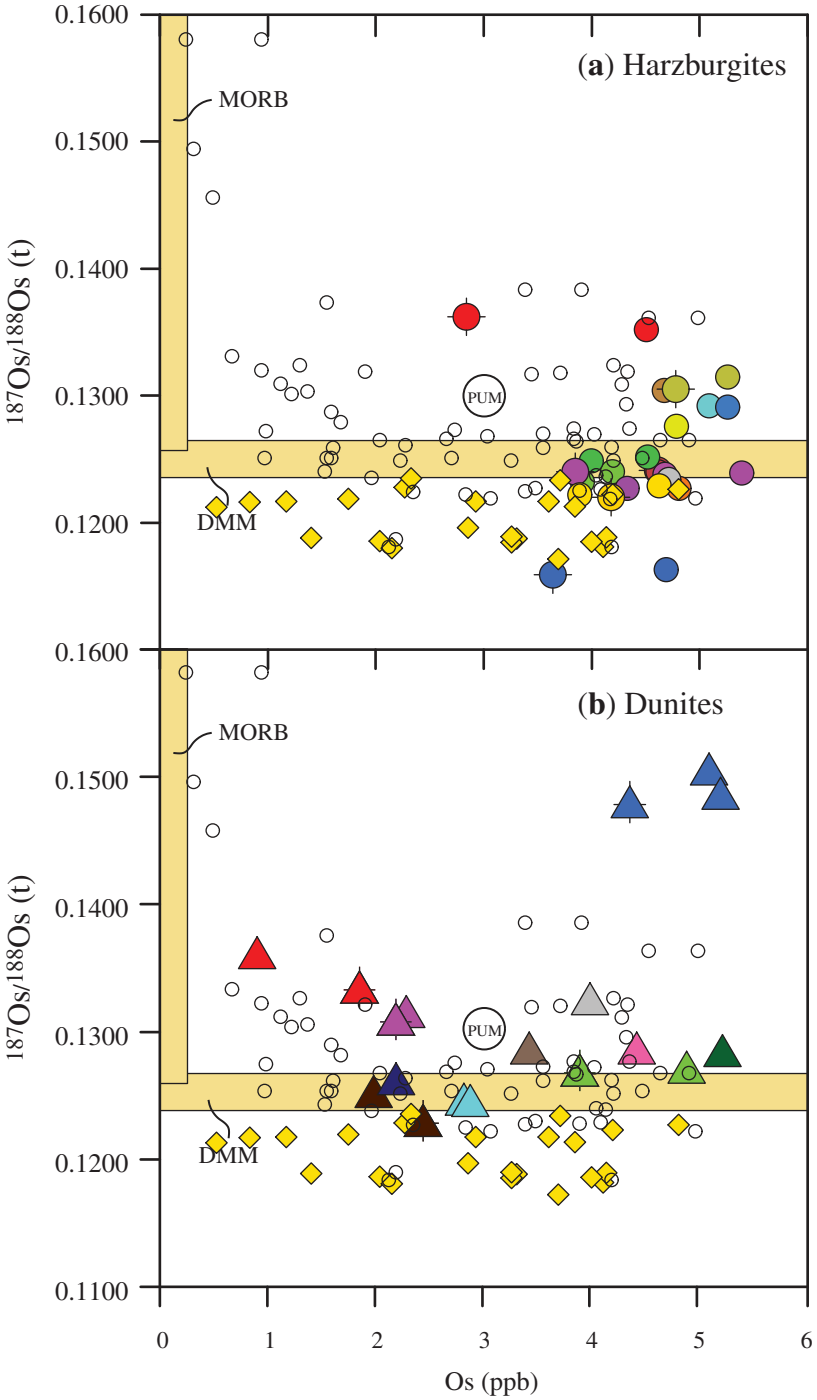

Fig. 8. Os isotope data at 90 Ma for Oman peridotites compared with abyssal peridotites, MORB and estimates of depleted MORB mantle (DMM), and primitive upper mantle (PUM), For both harzburgites (a) and dunites (b), samples are color coded to show replicate analyses [i.e. three blue symbols in (b) are replicate Os analyses of dunite sample OM94-52d]. Barbed symbols are Carius tube digestions and TIMS analyses from Harvard University; regular circles and triangles are flux fusion and sparging analyses from Woods Hole Oceanographic Institution (WHOI). Age correction is based on available Re analyses (no duplicates were run for Re concentration; see Table 6 for data). Abyssal peridotite data from Roy-Barman & Allègre (1994), Snow & Reisberg (1995), Brandon *et al.* (2000) and Standish *et al.* (2002) (open circles for all), and Harvey *et al.* (2006) (yellow diamonds); MORB data from Gannoun *et al.* (2004); DMM data from Snow & Reisberg (1995); PUM data from Meisel *et al.* (1996) and Walker *et al.* (2002).

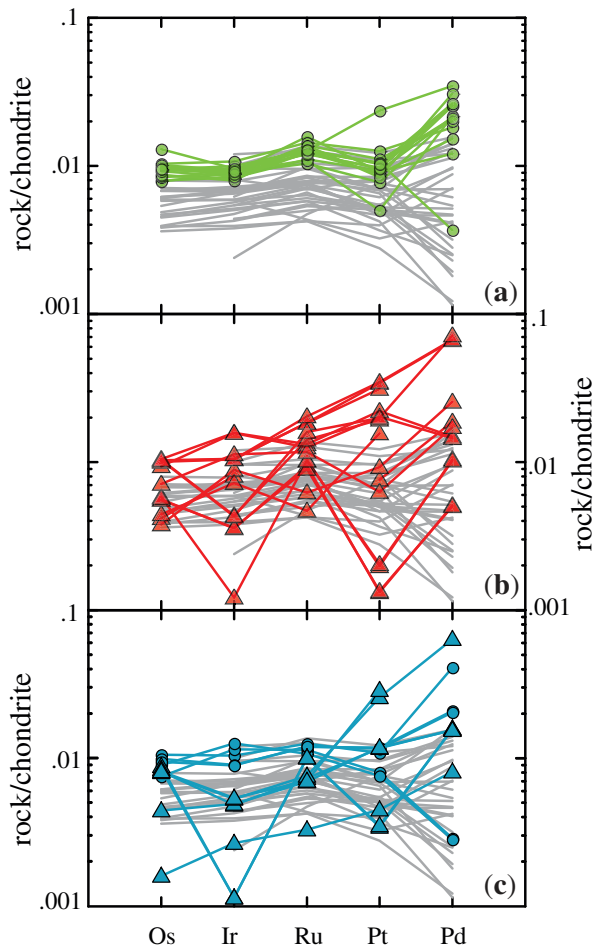

Fig. 9. Cl chondrite normalized (McDonough & Sun, 1995) PGE abundances compared with abyssal peridotites for (a) harzburgites, (b) dunites and (c) re-enriched samples. Abyssal peridotite data from Rehkamper *et al.* (1997), Snow & Schmidt (1998) and Luguet *et al.* (2003).

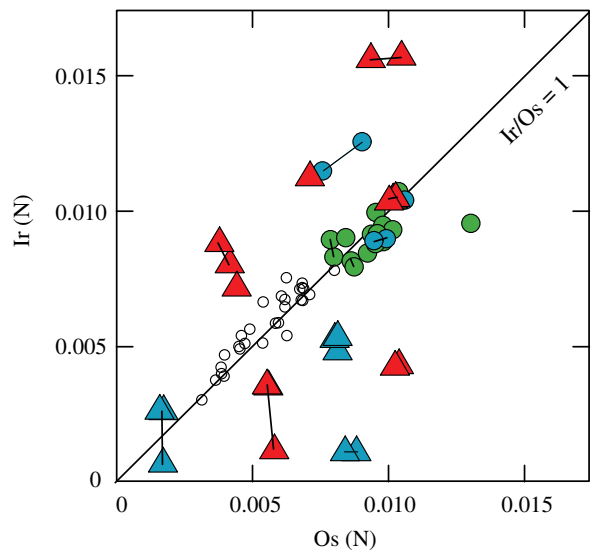

Fig. 10. Ir vs Os. Tie-lines connect duplicate analyses. Abyssal peridotite data (open circles) from Rehkamper *et al.* (1997), Snow & Schmidt (1998), and Luguet *et al.* (2003). Symbols as in Fig. 2.

Navon & Stolper (1987) emphasized a possible role for trace element fractionation during reactive porous flow of melt through residual peridotites; this type of process has been extensively modeled subsequently (e.g. review by Bodinier & Godard, 2003). Working specifically to explain the composition of peridotites from the Samail and Wadi Tayin massifs, Godard *et al.* (2000) showed that relative enrichment of REE in the main harzburgitic sequence can be successfully modeled with reactive porous flow at increasing melt mass with small amounts of trapped melt, and Bodinier & Godard (2003) pursued this line of reasoning further. Niu (2004) emphasized that in mid-ocean ridge peridotite samples, whole-rock REE patterns show more LREE enrichment, and sometimes even higher LREE concentrations, than clinopyroxenes in the same samples, and proposed that enrichment in highly incompatible elements is ubiquitous beneath spreading ridges from which peridotites have been sampled, and occurs via late, disequilibrium melt flow, crystallization ('impregnation') and reaction along crystal grain boundaries. Alternatively, Gruau *et al.* (1998) and Takazawa *et al.* (2003) proposed that U-shaped patterns might arise during alteration of depleted residual peridotites.

The enrichments of highly incompatible elements in our Oman samples are smaller than in the Niu dataset for mid-ocean ridge peridotites. Some of our samples record re-enrichment, consistent with impregnation with intergranular plagioclase, whose presence in highly depleted harzburgites is almost certainly due to partial crystallization of cooling melt migrating along grain boundaries in a depleted residue. However, most of our samples do not contain any evidence for impregnation, and our harzburgite samples have major element and HREE concentrations that are consistent with a simple origin as residues of melt extraction. If 'cryptic' re-fertilization in the shallow mantle beneath ridges is the process responsible for the U-shaped patterns, why would it be ubiquitous in all residual mantle samples, and of similar extent in the residues as evidenced by the roughly parallel patterns?

Instead, we favor the relatively new idea that enrichment of highly incompatible elements along grain boundaries in peridotite may be the result of near-equilibrium partitioning between grain boundaries and grain interiors (Hiraga *et al.*, 2004; Johnston & Schwab, 2004; Hiraga & Kohlstedt, 2007*a*, 2007*b*), rather than disequilibrium processes such as re-fertilization. Because grain boundaries a few microns wide constitute less than 1% of the volume of

a rock with millimeter-sized crystals, this effect becomes important only when equilibrated grain boundaries have trace element concentrations that are hundreds to thousands of times higher than in crystal interiors. Although the picture is undoubtedly complicated by impregnation in some samples, we think that the grain boundary partitioning hypothesis best explains the fact that the Oman harzburgites are more depleted in all incompatible trace elements, from HREE to large ion lithophile elements such as Cs, Rb and Ba, compared with oceanic peridotites, whereas both groups show roughly parallel, U-shaped REE patterns. Detailed work on partitioning between grain interiors and boundaries, along with very detailed grain size analyses, would be needed to fully test this hypothesis.

Distinctive dunite geochemistry: conduits for focused porous flow of MORB

In general, the lower abundance of incompatible trace elements in Wadi Tayin dunites relative to harzburgites reflects the primary modal mineralogy, with relatively trace element-rich orthopyroxene making up 20% of the harzburgites, but being essentially absent in dunites. The harzburgites and dunites all have a few per cent spinel. There is dramatic outcrop-scale variability in spinel abundance, especially in dunites, which can host 'chromitite bands' composed of almost 100% chromian spinel, varying in thickness from millimeters to meters. However, spinel abundance in general may be slightly lower in dunite compared with harzburgite. In our samples, harzburgites are generally richer in Ti than dunites, suggesting that orthopyroxene rather than spinel is the primary reservoir for Ti in these highly depleted residues. Nb and Ta concentrations are comparable in harzburgite and dunite, and thus these elements may be primarily hosted in spinel (or on grain boundaries) in both of these rock types.

In an important exception to the control of trace element abundances by the modal proportions of minerals in our samples, the range of LREE concentrations is the same in dunites and harzburgites. Thus, the dunites have high LREE/HREE ratios compared with the harzburgites. This is seen more clearly in mineral trace element data (Kelemen *et al.*, 1995; Braun, 2004), in which REE concentrations in rare clinopyroxenes in dunites are consistent with equilibrium with primitive, MORB-like melts like those that form the Oman crustal section, whereas REE in harzburgite clinopyroxenes reflect equilibration with a strongly LREE-depleted melt composition, consistent with that of late instantaneous liquids formed by high degrees of near fractional melting. We interpret the contrasting characteristics of dunites to be a consequence of highly focused flow of aggregated, MORB-like melts within high-porosity, dunite conduits, preserving major and trace element disequilibrium between these aggregated melts and surrounding harzburgites.

Pb enrichment correlated with Th, Nb, La and Ce enrichment

In the MORB-normalized trace element diagram (Fig. 3), all of our samples have striking U and Pb enrichment, and most samples also show large Sr enrichments. Similar enrichments are observed in mid-ocean ridge peridotite samples. The presence of relatively high Sr contents in harzburgites and re-enriched samples (including some dunites)—but not in most Oman dunites—suggests that high Sr is due to the presence of tiny amounts of plagioclase, and/or that Sr is retained in residues by orthopyroxene, with an unexpectedly high distribution coefficient during melting. There is no correlation between Eu and Sr, however, and more detailed mineralogical work would be needed to constrain the host phase(s) for Sr. This is probably complicated by trace amounts of Sr-bearing carbonate formed during alteration, although there is no correlation between Sr and LOI.

The presence of high U concentrations, relative to Th, is probably due to alteration. We base this not on the Oman dataset, but on the observation that dredged mid-ocean ridge peridotites have extensive, rusty weathering products including clay minerals and carbonate, and have extremely high U/Th (Niu, 2004), whereas drilled mid-ocean ridge peridotites from below the oxidized weathering horizon are greenish rather than rusty colored, generally lack carbonate, and have near-chondritic U/Th (M. Godard *et al.*, 2009, pesonal communication; Paulick *et al.*, 2006).

The presence of high Pb contents, relative to Ce and La, in all of our Oman peridotite samples and in all mid-ocean ridge peridotites (Niu, 2004) is a fascinating enigma. We initially thought that high Pb might be hosted in either 'impregnated' plagioclase or secondary carbonate. However, both plagioclase and carbonate in peridotites have high Sr concentrations, whereas Pb and Pb/Ce in our Oman dataset, and in mid-ocean ridge peridotites, do not correlate with Sr or Sr/Nd.

Another option is that Pb is hosted in sulfide minerals. Sulfides in ophiolite peridotites can have different origins. They can be a residual solid phase during mantle melting, they can crystallize from dense sulfide melt retained in residual peridotites, they can precipitate during melt–rock reaction, or they can form during hydrothermal alteration (e.g. Ahmed & Arai, 2002; Bockrath *et al.*, 2004; Alard *et al.*, 2005). Both primary and hydrothermal sulfide are known to be present in Oman peridotite samples (e.g. Ahmed & Arai, 2002). There is no correlation between Pb concentration and S concentration (not shown). However, correlations of Pb concentration with other trace elements cast doubt on the possibility that Pb is hosted primarily in sulfide.

If Pb were hosted in dense sulfide melt or solid phase sulfide retained in residual peridotites during silicate melt

extraction, one might expect Pb to behave as a compatible or only moderately incompatible element. Indeed, as one would expect from this scenario, Pb/Th, Pb/Ce and Pb/La ratios in our data and in mid-ocean ridge peridotites are negatively correlated with almost all incompatible element concentrations. In other words, the more depleted the sample, the higher the relative Pb enrichment. However, if Pb behaved as a compatible or moderately incompatible element during melt extraction, one would predict that Pb concentration would correlate best with Ni, Cr or HREE concentrations in these datasets, and/or that the least variable trace element ratios would be Pb/Ni, Pb/Cr, or Pb/HREE. Instead, among all the trace elements measured in the Oman peridotites and mid-ocean ridge peridotites, Pb concentrations correlate best with Th, Ce, La and Pr concentrations. [Correlation coefficients in the Niu (2004) dataset for mid-ocean ridge peridotites are Pb/Th 0·98, Pb/Ce 0·97, Pb/La 0·93, Pb/Pr 0·85, Pb/Nb 0·82, Pb/Ta 0·62.] The least variable ratios in the combined Wadi Tayin and mid-ocean ridge dataset are Pb/Ba, Pb/Th and Pb/La. These are not the characteristics that one would predict if Pb were compatible or moderately incompatible during melt extraction. Similarly, the high correlation coefficients for Pb with Th, Ce, La, Pr, Nb and Ta are not compatible with Pb enrichment via hydrothermal alteration. Th, Nb and Ta, in particular, are generally regarded as the trace elements in igneous rocks that are the least soluble in aqueous fluids, and therefore are least subject to hydrothermal alteration (Brenan *et al.*, 1995; Stalder *et al.*, 1998).

In summary, most traditional explanations for Pb enrichment do not seem to fit the data particularly well. It is unlikely that Pb is hosted in 'impregnated' plagioclase or hydrothermal carbonate, because Pb enrichment is not correlated with Sr enrichment. It is also unlikely that Pb is enriched in a residual sulfide phase, because the Pb systematics are not those of a compatible to moderately incompatible element. Finally, it is unlikely that Pb was enriched via hydrothermal alteration, because Pb concentrations correlate most strongly with the concentrations of trace elements thought to be least mobile during hydrothermal alteration. As a result, the origin of the Pb enrichments in these and similar peridotites remains somewhat enigmatic. One possibility, compatible with all the data, is that Pb is enriched via equilibrium partitioning between crystals and grain boundaries during melting and melt extraction, as proposed for highly incompatible elements in general by Hiraga *et al.* (2004) and Niu (2004). This would explain why Pb concentration is so closely correlated with highly incompatible trace elements, such that—although it is enriched relative to La and Ce in all samples—its concentration is lowest in low La samples and highest in high La samples. In essence, Pb in our samples and in mid-ocean ridge peridotites behaves like Th and Ba, and a similar explanation must be sought for enrichments in all three elements.

Osmium isotopes and PGE geochemistry

The osmium isotopic composition and PGE concentrations of these depleted mantle peridotites record substantial variability. An important observation is the more radiogenic nature of the dunites and impregnated peridotites compared with the residual harzburgites, and this may be due to relatively high $^{187}Os/^{188}Os$ in melt transported through the dunites. A similar interpretation has been proposed by Becker *et al.* (2001) for dunites in the Bohemian Massif, and by Buchl *et al.* (2002) for dunites in the Troodos ophiolite. This suggests that melt–rock ratios were high within the dunites (high enough to reset the isotope ratio for a compatible or moderately incompatible element), and that a significant proportion of the Os in the Oman mantle source was derived from a component with a distinctly more radiogenic Os composition than the ubiquitous depleted peridotite component represented by the residual harzburgite.

Data from mid-ocean ridges suggest that MORB glasses are also more radiogenic in Os than abyssal peridotites (e.g. Roy-Barman & Allègre, 1994; Snow & Reisberg, 1995; Schiano *et al.*, 1997; Alard *et al.*, 2005), although there is some debate about this. Alard *et al.* (2005) showed that igneous sulfides in abyssal peridotites have a wide range of Os isotopic compositions, including values comparable with MORB. However, radiogenic compositions in some abyssal peridotites may be a seawater alteration effect (e.g. Snow & Reisberg, 1995). An isotopic difference between residual peridotite and MORB, probably not related to seawater alteration, has also been proposed on the basis of Nd isotopic compositions (Salters & Dick, 2002).

The radiogenic sulfides described by Alard *et al.* (2005) are exclusively found in late-stage, texturally distinct, patches of clinopyroxene and spinel. These patches are interpreted as the result of reaction between residual peridotite and cooling, crystallizing melt entering the thermal boundary layer, and are therefore not a residual signature. Pb and Nd isotope data on clinopyroxene from abyssal peridotite are also consistent with an enriched component (radiogenic Pb, unradiogenic Nd) hosted in late, impregnated clinopyroxenes, and a depleted component hosted in older, matrix pyroxenes (Warren *et al.*, 2003, 2009). The presence of residual peridotites with whole-rock osmium isotopic compositions less radiogenic than MORB may be explained by melting of a heterogeneous (upwelling) mantle. Such a mantle would form mixed melts, in which much of the Os derives from areas (veins?) with high Re/Os in a matrix of previously depleted peridotite, thus giving rise to residual peridotites less radiogenic than the melts they formed.

Our Oman harzburgite samples have PGE abundances comparable with the most PGE-enriched abyssal peridotites, which is consistent with the PGE acting as compatible elements that are enriched in residues of relatively high degrees of melting. PGE abundances are generally lower and more variable in dunites compared with harzburgites, but they are still mostly within the range defined by abyssal peridotites. However, dunite Os/Ir ratios are highly variable, ranging from 0·5 to 8·3, whereas harzburgites and abyssal peridotites have Os/Ir ratios clustering tightly around unity (Fig. 10).

The Os/Ir ratios in dunites do not correlate with Os isotopic composition, abundance of any of the PGE or sulfur concentration. Although we have made several replicate analyses of PGE in dunites, the variability of the dunite data might have resulted from incomplete dissolution during analysis, or a nugget effect reflecting small-scale inhomogeneous distribution of ultra-trace PGE host phases. Preliminary mineral analyses indicate that sulfides in the peridotites have variable Os/Ir ratios, and we speculate that Os/Ir fractionation in the dunites is controlled by igneous sulfides during melt extraction. This may arise because dunites are not simply just residues of partial melting, but instead form by reaction between decompressing melt and residual mantle peridotite. We assume that dense sulfide melt remains within the solid residue of silicate melt extraction during mantle melting. Because sulfur concentration in sulfide-saturated melt increases with decreasing pressure (Mavrogenes & O'Neill, 1999; Holzheid & Grove, 2002), decompressing melts will dissolve some of the residual sulfide as they react with the surrounding peridotite, lowering residual sulfide concentration in dunites relative to host harzburgites. Assuming that PGE in peridotite are mainly hosted in sulfide (e.g. Hart & Ravizza, 1996; Alard *et al.*, 2005), and that the solubility of PGE in silicate melt is proportional to the sulfur concentration, this process should yield lower PGE concentrations in dunite compared with harzburgites.

From this point of view, the lack of correlation between sulfur and PGE concentrations in our samples may be due to the presence of low-PGE, secondary sulfide minerals formed during alteration. Alternatively, perhaps a significant amount of PGE are hosted in non-sulfide phases such as metals or alloys. Very detailed work will be required in the future to determine the relative importance of igneous and hydrothermal processes in producing the variability in PGE abundances observed in our Oman dunite samples.

High cooling rates and enriched incompatible elements in the uppermost mantle

Dynamically, probably the most important result of this study is that the shallowest samples are re-fertilized (i.e. anomalously enriched in incompatible elements), and record relatively high metamorphic closure temperatures. These observations suggest that migrating melt underwent crystallization during rapid cooling in the uppermost mantle during and immediately after ridge magmatism. A similar conclusion was reached by Ceuleneer *et al.* (1988) and Takazawa *et al.* (2003) on the basis of microstructural analyses.

Ca-in-orthopyroxene, Ca–Mg exchange between olivine and clinopyroxene (Kohler & Brey, 1990), Cr–Al exchange between orthopyroxene and spinel (Witt-Eickschen & Seck, 1991), and Fe–Mg exchange between olivine and spinel (Sack & Ghiorso, 1991; M. S. Ghiorso, 2007, pesonal communication) all confirm that the stratigraphically highest harzburgites equilibrated at higher temperatures than the deeper ones (Fig. 7). The correlation of the different thermometers involving distinct mineral pairs probably rules out systematic bias in the thermometry as a result of variations in bulk composition. Instead, the systematic decrease in closure temperature with increasing depth below the Moho transition zone probably reflects systematic variation in cooling rate as a function of depth in the mantle section.

A greater role for convecting fluids in the lower crust, perhaps extending into the uppermost mantle, compared with the deeper part of the section could explain these observations. In this context, perhaps the Moho Transition Zone acts as a permeability barrier during near-axis hydrothermal cooling. For example, the solid volume increase associated with serpentinization at Moho pressures could fill and seal porosity, preventing penetration of significant fluids to greater depth. In contrast, thermal contraction of plagioclase in cooling lower crustal gabbros may facilitate active hydrothermal convection extending to the Moho (Bosch *et al.*, 2004; Nicolas & Mainprice, 2005).

We hypothesize that the re-fertilization and higher closure temperatures recorded in the uppermost mantle samples are linked. More rapid cooling led to higher closure temperatures, and to partial crystallization of migrating melts in the shallowest part of the mantle section, yielding slightly elevated abundances of elements such as Ca and Na, and incompatible trace elements.

ACKNOWLEDGMENTS

This project has benefited tremendously from the analytical and scientific help and advice of Roberta Rudnick, Rick Carlson, Cinty Lee, Andy Saunders, Neel Chatterjee, Bernhard Peucker-Ehrenbrink, Jurek Blusztajn, Nobu Shimizu, Henry Dick, Jessica Warren, Anna Cipriani, Mike Braun, Greg Hirth and many others. Very helpful and constructive reviews were

provided by L. Reisberg, E. Takazawa and S. Shirey. This research was supported by OCE-0520391 and EAR-0337677 to P.B.K. and by the Cecil and Ida Green Postdoctoral Fellowship at WHOI and NSF Postdoctoral Fellowship EAR-9805684 to D.H.

REFERENCES

Ahmed, A. H. & Arai, S. (2002). Unexpectedly high-PGE chromitite from the deeper mantle section of the northern Oman ophiolite and its tectonic implications. *Contributions to Mineralogy and Petrology* **143**, 263–278.

Ahmed, A. H., Hanghøj, K., Kelemen, P. B., Hart, S. R. & Arai, S. (2006). Osmium isotope systematics of proterozoic and phanerozoic ophiolitic chromitites: in-situ ion probe analysis of primary Os-rich PGM. *Earth and Planetary Science Letters* **245**, 771–791.

Alabaster, T., Pearce, J. A. & Malpas, J. (1982). The volcanic stratigraphy and petrogenesis of the Oman ophiolite complex. *Contributions to Mineralogy and Petrology* **81**, 168–183.

Alard, O., Luguet, A., Pearson, N. J., Griffin, W. L., Lorand, J.-P., Gannoun, A., Burton, K. W. & O'Reilly, S. Y. (2005). *In situ* Os isotopes in abyssal peridotites bridge the isotopic gap between MORBs and their source mantle. *Nature* **436**, 1005–1008.

Amri, I., Benoit, M. & Ceuleneer, G. (1996). Tectonic setting for the genesis of oceanic plagiogranites: evidence from a paleo-spreading structure in the Oman ophiolite. *Earth and Planetary Science Letters* **139**, 177–194.

Arai, S. (1994). Characterization of spinel peridotites by olivine–spinel compositional relationships: Review and interpretation. *Chemical Geology* **113**, 191–204.

Arai, S., Uesugi, J. & Ahmed, A. H. (2004). Upper crustal podiform chromitite from the northern Oman ophiolite as the stratigraphically shallowest chromitite in ophiolite and its implication for Cr concentration. *Contributions to Mineralogy and Petrology* **147**, 145–154.

Augé, T. (1987). Chromite deposits in the northern Oman ophiolite: Mineralogical constraints. *Mineralium Deposita* **22**, 1–10.

Becker, H., Shirey, S. B. & Carlson, R. W. (2001). Effects of melt percolation on the Re–Os systematics of peridotites from a Paleozoic convergent plate margin. *Earth and Planetary Science Letters* **188**, 107–121.

Benoit, M., Polve, M. & Ceuleneer, G. (1996). Trace element and isotopic characterization of mafic cumulates in a fossil mantle diapir (Oman ophiolite). *Chemical Geology* **134**, 199–214.

Benoit, M., Ceuleneer, G. & Polvé, M. (1999). The remelting of hydrothermally altered peridotite at mid-ocean ridges by intruding mantle diapirs. *Nature* **402**, 514–518.

Bockrath, C. B., Ballhaus, C. & Holzheid, A. H. (2004). Fractionation of the platinum-group elements during mantle melting. *Science* **305**, 1951–1953.

Bodinier, J.-L. & Godard, M. (2003). Orogenic, ophiolitic, and abyssal peridotites. In: Carlson, R.W. (ed.) *Treatise on Geochemistry, Volume 2, The Mantle and Core*. Oxford: Elsevier-Pergamon, pp. 103–170.

Bosch, D., Jamais, M., Boudier, F., Nicolas, A., Deutzia, J. M. & Grimier, P. (2004). Deep and high-temperature hydrothermal circulation in the Oman ophiolite—metrological and isotopic evidence. *Journal of Petrology* **45**, 1181–1208.

Boudier, F. & Coleman, R. G. (1981). Cross section through the peridotite in the Samail ophiolite, southeastern Oman mountains. *Journal of Geophysical Research* **86**, 2573–2592.

Boudier, F., Godard, M. & Ambusher, C. (2000). Significance of gabbronorite occurrence in the crustal section of the Samail Ophiolite. *Marine Geophysical Researches* **21**, 307–326.

Brandon, A. D., Snow, J., Walker, R. J., Morgan, J. W. & Mock, T. D. (2000). ^{190}Pt–^{186}Os and ^{187}Re–^{187}Os systematics of abyssal peridotites. *Earth and Planetary Science Letters* **177**, 319–335.

Braun, M. G. (2004). Petrological and microstructural constraints on focused melt transport in dunites and rheology of the shallow mantle. MIT–WHOI joint graduate program thesis, 212 pp.

Braun, M. G. & Kelemen, P. B. (2001). Mapping dunite melt conduits in the mantle: Constraints on dunite formation and MORB flux. *EOS Transactions, American Geophysical Union* **82**, S431.

Braun, M. G. & Kelemen, P. B. (2002). Dunite distribution in the Oman Ophiolite: Implications for melt flux through porous dunite conduits. *Geochemistry, Geophysics, Geosystems* **3**(11), 8603, doi:10.1029/2001GC000289.

Brenan, J. M., Shaw, H. F., Ryerson, F. J. & Phinney, D. L. (1995). Mineral–aqueous fluid partitioning of trace elements at 900°C and 2·0 GPa: constraints on the trace element chemistry of mantle and deep crustal fluids. *Geochimica et Cosmochimica Acta* **59**, 3331–3350.

Brey, G. P. & Kohler, T. (1990). Geothermobarometry in four-phase lherzolites II. New thermobarometers, and the practical assessment of existing thermobarometers. *Journal of Petrology* **31**, 1353–1378.

Buchl, A., Brugmann, G., Batanova, V. G., Munker, C. & Hofmann, A. W. (2002). Melt percolation monitored by Os isotopes and HSE abundances: A case study from the mantle section of the Troodos Ophiolite. *Earth and Planetary Science Letters* **204**, 385–402.

Ceuleneer, G., Nicolas, A. & Boudier, F. (1988). Mantle flow patterns at an oceanic spreading center—the Oman Ophiolite. *Tectonophysics* **151**(1–4), 1–26.

Chatterjee, N., Bhattacharji, S. & Fein, C. (2005). Depth of alkalic magma reservoirs below Kolekole cinder cone, Southwest rift zone, East Maui, Hawaii. *Journal of Volcanology and Geothermal Research* **145**, 1–22.

Creaser, R. A., Papanastassiou, D. J. & Wasserburg, G. J. (1991). Negative thermal ion spectrometry of osmium, rhenium and iridium. *Geochimica et Cosmochimica Acta* **55**, 397–401.

Dick, H. J. B. (1977). Partial melting in the Josephine Peridotite; I, The effect on mineral composition and its consequence for geobarometry and geothermometry. *American Journal of Science* **277**, 801–832.

Dick, H. J. B. (1989). Abyssal peridotites, very slow spreading ridges, and ocean ridge magmatism. In: Saunders, A. D. & Norry, M. J. (eds) *Magmatism in the Ocean Basins. Geological Society, London, Special Publications* **42**, 71–105.

Dick, H. J. B. & Bullen, T. (1984). Chromian spinel as a petrogenetic indicator in abyssal and alpine-type peridotites and spatially associated lavas. *Contributions to Mineralogy and Petrology* **86**, 54–76.

Dick, H. J. B. & Natland, J. H. (1996). Late-stage melt evolution and transport in the shallow mantle beneath the East Pacific Rise. In: Mevel, C., Gillis, K. M., Allan, J. F. & Meyer, P. S. (eds) *Proceedings of the Ocean Drilling Program, Scientific Results, 147.* College Station, TX: Ocean Drilling Program, pp. 103–134.

Ernewein, M., Pflumio, C. & Whitechurch, H. (1988). The death of an accretion zone as evidenced by the magmatic history of the Sumail ophiolite (Oman). *Tectonophysics* **151**, 247–274.

Gannoun, A., Burton, K. W., Thomas, L. E., Parkinson, I. J. & van Calsteren, P. (2004). Osmium isotope heterogeneity in the constituent phases of mid-ocean ridge basalts. *Science* **303**, 70–72.

Garrido, C. J., Kelemen, P. B. & Hirth, G. (2001). Variation of cooling rate with depth in lower crust formed at an oceanic spreading ridge: Plagioclase crystal size distributions in gabbros from the

Oman ophiolite. *Geochemistry, Geophysics, Geosystems* **2**(10), 1041, doi:10.1029/2000GC000136.

Godard, M., Jousselin, D. & Bodinier, J.-L. (2000). Relationships between geochemistry and structure beneath a paleo-spreading centre; a study of the mantle section in the Oman Ophiolite. *Earth and Planetary Science Letters* **180**, 133–148.

Godard, M., Dautria, J.-M. & Perrin, M. (2003). Geochemical variability of the Oman ophiolite lavas: Relationship with spatial distribution and paleomagnetic directions. *Geochemistry, Geophysics, Geosystems* **4**(6), 8609, doi:10.1029/2002GC000452.

Godard, M., Lagabrielle, Y., Alard, O. & Harvey, J. (2008). Geochemistry of the highly depleted peridotites drilled at ODP Sites 1272 and 1274 (Fifteen-Twenty Fracture Zone, Mid-Atlantic Ridge): Implications for mantle dynamics beneath a slow spreading ridge. *Earth and Planetary Science Letters* **267**(3–4), 410–425, doi:10.1016/j.epsl.2007.11.058.

Gregory, R. T. (1984). Melt percolation beneath a spreading ridge: evidence from the Semail peridotite, Oman. In: Gass, I. G., Lippard, S. J. & Shelton, A. W. (eds) *Ophiolites and Oceanic Lithosphere. Geological Society, London, Special Publications* **13**, 55–62.

Gruau, G., Bernard-Griffiths, J. & Lecuyer, C. (1998). The origin of the U-shaped rare earth patterns in ophiolite peridotites: Assessing the role of secondary alteration and melt/rock reaction. *Geochimica et Cosmochimica Acta* **62**, 3545–3560.

Hacker, B. R., Mosenfelder, J. L. & Gnos, E. (1996). Rapid emplacement of the Oman Ophiolite; thermal and geochronologic constraints. *Tectonics* **15**, 1230–1247.

Hart, S. R. & Ravizza, G. E. (1996). Os partitioning between phases in lherzolite and basalt: Earth processes. In: Basu, A. & Hart, S. R. (eds) *Reading the Isotopic Code. Geophysical Monograph, American Geophysical Union* **95**, 123–134.

Harvey, J., Gannoun, A., Burton, K. W., Rogers, N. W., Alard, O. & Parkinson, I. J. (2006). Ancient melt extraction from the oceanic upper mantle revealed by Re–Os isotopes in abyssal peridotites from the Mid-Atlantic ridge. *Earth and Planetary Science Letters* **244**, 606–621.

Hassler, D. R., Peucker-Ehrenbrink, B. & Ravizza, G. E. (2000). Rapid determination of Os isotopic composition by sparging OsO_4 into a magnetic-sector ICP-MS. *Chemical Geology* **166**, 1–14.

Hauri, E. H. & Hart, S. R. (1993). Re–Os isotope systematics of HIMU and EMII oceanic island basalts from the south Pacific Ocean. *Earth and Planetary Science Letters* **114**, 353–371.

Hiraga, T. & Kohlstedt, D. L. (2007*a*). Equilibrium interface segregation in the diopside–forsterite system I: Analytical techniques, thermodynamics, and segregation characteristics. *Geochimica et Cosmochimica Acta* **71**(5), 1266–1280.

Hiraga, T. & Kohlstedt, D. L. (2007*b*). Equilibrium interface segregation in the diopside–forsterite system II: Applications of interface enrichment to mantle geochemistry. *Geochimica et Cosmochimica Acta* **71**(5), 1281–1289.

Hiraga, T., Anderson, I. M. & Kohlstedt, D. L. (2004). Partitioning in mantle rocks: grain boundaries as reservoirs of incompatible elements. *Nature* **427**, 699–703.

Hofmann, A. W. (1988). Chemical differentiation of the Earth: the relationship between mantle, continental crust, and oceanic crust. *Earth and Planetary Science Letters* **90**, 297–314.

Holtzman, B., Dilek, Y., Moores, E. M., Elthon, D. & Nicolas, A. (2000). Gauging stress from mantle chromitite pods in the Oman Ophiolite. In: Dilek, Y., Moores, E., Elthon, D. & Nicolas, A. (eds) Ophiolites and Oceanic Crust; New Insights from Field Studies and the Ocean Drilling Program: Penrose Conference on Ophiolites and Oceanic Crust; New Insights from Field Studies and the Ocean Drilling Program. *Geological Society of America Special Paper* **349**, pp. 149–158.

Holzheid, A. & Grove, T. L. (2002). Sulfur saturation limits in silicate melts and their implications for core formation scenarios for terrestrial planets. *American Mineralogist* **87**, 227–237.

Humler, E., Langmuir, C. & Daux, V. (1999). Depth versus age; new perspectives from the chemical compositions of ancient crust. *Earth and Planetary Science Letters* **173**, 7–23.

Ildefonse, B., Nicolas, A. & Boudier, F. (1993). Evidence from the Oman ophiolite for sudden stress changes during melt injection at oceanic spreading centres. *Nature* **366**, 673–675.

Ishikawa, T., Nagaishi, K. & Umino, S. (2002). Boninitic volcanism in the Oman ophiolite: Implications for thermal condition during transition from spreading ridge to arc. *Geology* **30**, 899–902.

Johnson, D. M., Hooper, P. R. & Conrey, R. M. (1999). XRF analysis of rocks and minerals for major and trace elements on a single low dilution Li-tetraborate fused bead. Advances in X-*ray* Analysis **41**, 843–867.

Johnson, K. T. & Dick, H. J. B. (1992). Open system melting and temporal and spatial variation of peridotite and basalt at the Atlantis II fracture zone. *Journal of Geophysical Research* **97**, 9219–9241.

Johnson, K. T., Dick, H. J. B. & Shimizu, N. (1990). Melting in the oceanic upper mantle: an ion microprobe study of diopsides in abyssal peridotites. *Journal of Geophysical Research* **95**, 2661–2678.

Johnston, A. D. & Schwab, B. E. (2004). Constraints on clinopyroxene/melt partitioning of REE, Rb, Sr, Ti, Cr, Zr, and Nb during mantle melting: First insights from direct peridotite melting experiments at 1·0 GPa. *Geochimica et Cosmochimica Acta* **68**, 4949–4962.

Juteau, T., Beurrier, M., Dahl, R. & Nehlig, P. (1988*a*). Segmentation at a fossil spreading axis: The plutonic sequence of the Wadi Haymiliyah area (Haylayn Block, Sumail Nappe, Oman). *Tectonophysics* **151**, 167–197.

Juteau, T., Ernewein, M., Reuber, I., Whitechurch, H. & Dahl, R. (1988*b*). Duality of magmatism in the plutonic sequence of the Sumail Nappe, Oman. *Tectonophysics* **151**, 107–135.

Kelemen, P. B. (1986). Assimilation of ultramafic rock in subduction-related magmatic arcs. *Journal of Geology* **94**, 829–843.

Kelemen, P. B. & Dick, H. J. B. (1995). Focused melt flow and localized deformation in the upper mantle: Juxtaposition of replacive dunite and ductile shear zones in the Josephine peridotite, SW Oregon. *Journal of Geophysical Research* **100**, 423–438.

Kelemen, P. B., Shimizu, N. & Salters, V. J. M. (1995). Extraction of mid-ocean ridge basalt from the upwelling mantle by focused flow of melt in dunite channels. *Nature* **375**, 747–753.

Kelemen, P. B., Hirth, G., Shimizu, N., Spiegelman, M. & Dick, H. J. B. (1997). A review of melt migration processes in the adiabatically upwelling mantle beneath oceanic spreading ridges. *Philosophical Transactions of the Royal Society of London, Series* **A 355**, 283–318.

Klein, E. M. & Langmuir, C. H. (1987). Global correlations of ocean ridge basalt chemistry with axial depth and crustal thickness. *Journal of Geophysical Research* **92**, 8089–8115.

Koga, K. T., Kelemen, P. B. & Shimizu, N. (2001). Petrogenesis of the crust–mantle transition zone and the origin of lower crustal wehrlite in the Oman ophiolite. *Geochemistry, Geophysics, Geosystems* **2**(9), 1038, doi:10.1029/2000GC000132.

Kohler, T. P. & Brey, G. P. (1990). Calcium exchange between olivine and clinopyroxene calibrated as a geothermobarometer. *Geochimica et Cosmochimica Acta* **54**, 2375–2388.

Korenaga, J. & Kelemen, P. B. (1997). Origin of gabbro sills in the Moho transition zone of the Oman ophiolite: Implications for magma transport in the oceanic lower crust. *Journal of Geophysical Research* **102**, 27, 27729–27749.

Lachize, M., Lorand, J. P. & Juteau, T. (1996). Calc-alkaline differentiation trend in the plutonic sequence of the Wadi Haymiliyah section, Haylayn massif, Semail ophiolite, Oman. *Lithos* **38**, 207–232.

Langmuir, C. H., Klein, E. M. & Plank, T. (1992). Petrological systematic of mid-ocean ridge basalts: Constraints on melt generation beneath ocean ridges. In: Morgan, J. P., Blackman, D. K. & Sinton, J. M. (eds) *Mantle Flow and Melt Generation beneath Mid-ocean Ridges. Geophysical Monograph, American Geophysical Union* **71**, 183–281.

Lee, C. T., Yin, Q. Z., Rudnick, R. L., Chesley, J. T. & Jacobsen, S. B. (2000). Osmium isotopic evidence for Mesozoic removal of lithospheric mantle beneath the Sierra Nevada, California. *Science* **289**, 1912–1916.

Le Mée, L., Girardeau, J. & Monnier, C. (2004). Mantle segmentation along the Oman ophiolite fossil mid-ocean ridge. *Nature* **432**, 167–172.

Lippard, S. J., Shelton, A. W. & Gass, I. G. (1986). *The Ophiolite of Northern Oman*. Oxford: Blackwell, 178 p.

Lorand, J. P. & Ceuleneer, G. (1989). Silicate and base-metal sulfide inclusions in chromites from the Maqsad area (Oman ophiolite, Gulf of Oman): A model for entrapment. *Lithos* **22**, 173–190.

Luguet, A., Lorand, J. P. & Seyler, M. (2003). Sulfide petrology and highly siderophile element geochemistry of abyssal peridotites: A coupled study of samples from the Kane Fracture Zone (45°W, 23°20N, MARK Area, Atlantic Ocean). *Geochimica et Cosmochimica Acta* **67**, 1553–1570.

Mavrogenes, J. A. & O'Neill, H. St. C. (1999). The relative effects of pressure, temperature and oxygen fugacity on the solubility of sulfide in mafic magmas. *Geochimica et Cosmochimica Acta* **63**, 1173–1180.

McCulloch, M. T., Gregory, R. T., Wasserburg, G. J. & Taylor, H. P. (1981). Sm–Nd, Rb–Sr, and ^{18}O–^{16}O isotopic systematics in an oceanic crustal section—evidence from the Samail Ophiolite. *Journal of Geophysical Research* **86**, 2721–2735.

McDonough, W. F. & Sun, S.-s. (1995). The composition of the Earth. *Chemical Geology* **120**, 223–253.

Meisel, T., Walker, R. J. & Morgan, J. W. (1996). The osmium isotopic composition of the Earth's primitive upper mantle. *Nature* **383**, 517–520.

Monnier, C., Girardeau, J., Le Mée, L. & Polvé, M. (2006). Along-ridge petrological segmentation of the mantle in the Oman ophiolite. *Geochemistry, Geophysics, Geosystems* **7**, Q11008, doi:10.1029/2006GC001320.

Navon, O. & Stolper, E. (1987). Geochemical consequences of melt percolation; the upper mantle as a chromatographic column. *Journal of Geology* **95**, 285–307.

Nicolas, A. (1989). *Structure of Ophiolites and Dynamics of Oceanic Lithosphere*. Boston, MA: Kluwer Academic, 367 p.

Nicolas, A. & Boudier, F. (1995). Mapping oceanic ridge segments in Oman ophiolite. *Journal of Geophysical Research* **100**, 6179–6197.

Nicolas, A. & Boudier, F. (2001). Oman and UAE Ophiolite Map. *Marine Geophysical Research* **21**.

Nicolas, A. & Boudier, F. (2008). Large shear zones with no relative displacement. *Terra Nova* **20**, 200–205.

Nicolas, A. & Mainprice, D. (2005). Burst of high-temperature seawater injection throughout accreting oceanic crust: A case study in Oman ophiolite. *Terra Nova* **4**, 326–330.

Nicolas, A., Boudier, F. & Ildefonse, B. (1994). Evidence from the Oman ophiolite for active mantle upwelling beneath a fast-spreading ridge. *Nature* **370**, 51–53.

Nicolas, A., Boudier, F. & Ildefonse, B. (1996). Variable crustal thickness in the Oman Ophiolite; implication for oceanic crust. *Journal of Geophysical Research* **101**, 17941–17950.

Nicolas, A., Boudier, F., Ildefonse, B. & Ball, E. (2000). Accretion of Oman and United Arab Emirates ophiolite—Discussion of a new structural map. *Marine Geophysical Research* **21**, 147–179.

Niu, Y. (1997). Mantle melting and melt extraction processes beneath ocean ridges; evidence from abyssal peridotites. *Journal of Petrology* **38**, 1047–1074.

Niu, Y. (2004). Bulk-rock major and trace element compositions of abyssal peridotites: Implications for mantle melting, melt extraction and post-melting processes beneath mid-ocean ridges. *Journal of Petrology* **45**, 2423–2458.

Nonnotte, P., Ceuleneer, C. & Benoit, M. (2005). Genesis of andesitic–boninitic magmas at mid-ocean ridges by melting of hydrated peridotites: Geochemical evidence from DSDP Site 334 gabbronorites. *Earth and Planetary Science Letters* **236**, 632–653.

Pallister, J. S. (1981). Structure of the sheeted dike complex of the Samail ophiolite near Ibra, Oman. *Journal of Geophysical Research* **86**, 2661–1672.

Pallister, J. S. & Hopson, C. A. (1981). Samail ophiolite plutonic suite: field relations, phase variation, cryptic variation and layering, and a model of a spreading ridge magma chamber. *Journal of Geophysical Research* **86**, 2593–2644.

Pallister, J. S. & Knight, R. J. (1981). Rare-earth element geochemistry of the Samail ophiolite near Ibra, Oman. *Journal of Geophysical Research* **86**, 2673–2697.

Parkinson, I. J. & Pearce, J. A. (1998). Peridotites from the Izu–Bonin–Mariana Forearc (ODP Leg 125): Evidence for mantle melting and melt–mantle interaction in a supra-subduction zone setting. *Journal of Petrology* **39**, 1577–1618.

Paulick, H., Bach, W., Godard, M., De Hoog, J. M. C., Suhr, G. & Harvey, J. (2006). Geochemistry of abyssal peridotites (Mid-Atlantic Ridge, 15°20′N,ODP Leg 209): Implications for fluid/rock interaction in slow spreading environments. *Chemical Geology* **234**, 179–210.

Pearce, J. A., Alabaster, T., Shelton, A. W. & Searle, M. P. (1981). The Oman ophiolite as a Cretaceous arc-basin complex: Evidence and implications. *Philosophical Transactions of the Royal Society of London* **300**, 299–317.

Prinzhofer, A. & Allègre, C. J. (1985). Residual peridotites and the mechanisms of partial melting. *Earth and Planetary Science Letters* **74**, 251–265.

Python, M. & Ceuleneer, G. (2003). Nature and distribution of dykes and related melt migration structures in the mantle section of the Oman ophiolite. *Geochemistry, Geophysics, Geosystems* **4**(7), 8612, doi:10.1029/2002GC000354.

Ravizza, G. & Pyle, D. (1997). PGE and Os isotopic analyses of single sample aliquots with NiS fire assay preconcentration. *Chemical Geology* **141**, 251–268.

Rehkamper, M., Halliday, A. N., Barfod, D., Fitton, J. G. & Dawson, J. B. (1997). Platinum-Group element abundance patterns in different mantle environments. *Science* **278**, 1595–1598.

Reisberg, L., Allègre, C. J. & Luck, J.-M. (1991). The Re–Os systematics of the Ronda ultramafic complex of southern Spain. *Earth and Planetary Science Letters* **105**, 196–213.

Reisberg, L., Zindler, A., Marcantonio, F., White, W., Wyman, D. & Weaver, B. (1993). Os isotope systematics in ocean island basalts. *Earth and Planetary Science Letters* **120**, 149–167.

Reuber, I. (1988). Complexity of the crustal sequence in the northern Oman ophiolite (Fizh and southern Aswad blocks): The effect of early slicing? *Tectonophysics* **151**, 137–141.

Reuber, I., Nehlig, P. & Juteau, T. (1991). Axial segmentation at a fossil oceanic spreading centre in the Haylayn block (Semail nappe, Oman): off-axis mantle diapir and advancing ridge tip. *Journal of Geodynamics* **13**, 253–278.

Ross, K. & Elthon, D. (1993). Cumulates from strongly depleted mid-ocean-ridge basalt. *Nature* **365**, 826–829.

Roy-Barman, M. & Allègre, C. J. (1994). $^{187}Os/^{186}Os$ ratios of mid-ocean ridge basalts and abyssal peridotites. *Geochimica et Cosmochimica Acta* **58**, 5043–5054.

Sack, R. O. & Ghiorso, M. S. (1991). Chromian spinels as petrogenetic indicators; thermodynamics and petrological applications. *American Mineralogist* **76**, 827–847.

Salters, V. J. M. & Dick, H. J. B. (2002). Mineralogy of the mid-ocean-ridge basalt source from neodymium isotopic composition of abyssal peridotites. *Nature* **418**, 68–72.

Schiano, P., Birck, J.-L. & Allègre, C. J. (1997). Osmium–strontium–neodymium–lead isotopic covariations in mid-ocean ridge basalt glasses and the heterogeneity of the upper mantle. *Earth and Planetary Science Letters* **150**, 363–379.

Sharma, M. & Wasserburg, G. J. (1996). The neodymium isotopic compositions and rare earth patterns in highly depleted ultramafic rocks. *Geochimica et Cosmochimica Acta* **60**(22), 4537–4550.

Shirey, S. B. & Walker, R. J. (1995). Carius tube digestion for low-blank rhenium–osmium analysis. *Analytical Chemistry* **67**, 2136–2141.

Smewing, J. D. (1981). Mixing characteristics and compositional differences in mantle-derived melts beneath spreading axes: Evidence from cyclically layered rocks in the ophiolite of North Oman. *Journal of Geophysical Research* **86**, 2645–2659.

Snow, J. E. & Reisberg, L. (1995). Erratum of 'Os isotopic systematics of the MORB mantle: results from altered abyssal peridotites'. *Earth and Planetary Science Letters* **136**, 723–733.

Snow, J. E. & Schmidt, G. (1998). Constraints on Earth accretion deduced from noble metals in the oceanic mantle. *Nature* **391**, 166–169.

Stalder, R., Foley, S. F., Brey, G. P. & Horn, I. (1998). Mineral–aqueous fluid partitioning of trace elements at 900–1200°C and 3·0–5·7 GPa: New experimental data for garnet, clinopyroxene, and rutile, and implications for mantle metasomatism. *Geochimica et Cosmochimica Acta* **62**, 1781–1801.

Standish, J. J., Hart, S. R., Blusztajn, J., Dick, H. J. B. & Lee, K. L. (2002). Abyssal peridotite osmium isotopic compositions from Cr-spinel. *Geochemistry, Geophysics, Geosystems* **3**(1), 1004, doi:10.1029/2001GC000161.

Sun, S. S. & McDonough, W. F. (1989). Chemical and isotopic systematics of oceanic basalts; implications for mantle composition and processes. In: Saunders, A. D. & Norry, M. J. (eds) *Magmatism in the Ocean Basins. Geological Society, London, Special Publications* **42**, 313–345.

Takazawa, E., Okayasu, T. & Satoh, K. (2003). Geochemistry and origin of the basal lherzolites from the northern Oman ophiolite (northern Fizh block). *Geochemistry, Geophysics, Geosystems* **4**(2)), doi:10.1029/2001GC000232.

Tilton, G. R., Hopson, C. A. & Wright, J. E. (1981). Uranium–lead isotopic ages of the Samail ophiolite, Oman, with applications to tethyan ocean ridge tectonics. *Journal of Geophysical Research* **86**, 2763–2775.

Volkening, J., Walczyk, T. & Heumann, K. (1991). Osmium isotope ratio determinations by negative thermal ionization mass spectrometry. *International Journal of Mass Spectrometry and Ion Processes* **105**, 147–159.

Walker, R. J., Prichard, H. M., Ishiwatari, A. & Pimentel, M. (2002). The osmium isotopic composition of convecting upper mantle deduced from ophiolite chromites. *Geochimica et Cosmochimica Acta* **66**(2), 329–345.

Warren, J. M., Shimizu, N. & Dick, H. J. B. (2003). Melt impregnation revealed by clinopyroxene geochemistry in abyssal peridotite. *Geochimica et Cosmochimica Acta* A526.

Warren, J. M., Shimizu, N., Sakaguchi, C., Dick, H. J. B. & Nakamura, E. (2009). An assessment of upper mantle heterogeneity based on abyssal peridotite isotopic compositions. *Journal of Geophysical Research* (in press).

Witt-Eickschen, G. & Seck, H. A. (1991). Solubility of Ca and Al in orthopyroxene from spinel peridotite: An improved version of an empirical geothermometer. *Contributions to Mineralogy and Petrology* **106**, 431–439.